Quantum Electronics **41** (4) 284–301 (2011)

PACS numbers: 42.70.Qs; 42.81.Bm; 42.62.Be
DOI: 10.1070/QE2011v041n04ABEH014536

Photonic crystal fibres in biomedical investigations

Yu.S. Skibina, V.V. Tuchin, V.I. Beloglazov, G. Steinmeyer,
J. Bethge, R. Wedell, N. Langhoff

Abstract. **The state of the art in the field of design and study of photonic crystal fibres for biomedical applications is considered and some original results recently obtained by the authors are presented. Optical properties of the fibres that offer prospects of their wide application as biological sensors, 'labs-on-a-chip', and facilities of electromagnetic radiation control in a wide range of wavelengths aimed at designing novel biomedical instrumentation are considered.**

Keywords: *photonic crystal fibre, biological sensors, nanobiophotonics.*

1. Introduction

Nanobiophotonics is the field of photonics, related to the design and technology of manufacturing nanostructure devices for generation, amplification, modulation, transmission and detection of electromagnetic radiation and instrumentation, using such devices for the purposes of biology and medicine. Nanobiophotonics also deals with the study of physical phenomena that determine the interaction of photons with nanoscale structures of both devices and biological objects.

At present a promising area of study is creating new materials for designing transducers with controllable optical response. Nanostructured materials offer new unique possibilities for biophotonics. The driving force of creating new nanostructured materials is, first of all, the understanding of their wide applicability and prospects of new discoveries in various fields of science and technology, including biology and medicine.

Yu.S. Skibina N.G. Chernyshevsky National Research Saratov State University, ul. Astrakhanskaya 83, 410012 Saratov, Russia; LLC SPE "Nanostructural Glass Technology", prosp. 50 let Oktyabrya 101, 410033 Saratov, Russia; e-mail: skibinajs@yandex.ru;
V.V. Tuchin N.G. Chernyshevsky National Research Saratov State University, ul. Astrakhanskaya 83, 410012 Saratov, Russia; Institute of Precision Mechanics and Control, Russian Academy of Sciences, ul. Rabochaya 24, 410028 Saratov, Russia; e-mail: tuchinvv@mail.ru;
V.I. Beloglazov LLC SPE "Nanostructural Glass Technology", prosp. 50 let Oktyabrya 101, 410033 Saratov, Russia; e-mail: beloglazovvi@yandex.ru;
G. Steinmeyer, J. Bethge Max-Born Institute, Germany, 12489 Berlin, Max-Born str. 2a; e-mail: steinmey@mbi-berlin.de, bethge@mbi-berlin.de;
R. Wedell Institute of Applied Photonics, Germany, 12489 Berlin, Rudower Chaussee 29/31; e-mail: wedell-iap@ifg-adlershof.de;
N. Langhoff Institute for Scientific Instruments GmbH, Germany, 12489 Berlin, Rudower Chaussee 29/31; e-mail: langhoff@ifg-adlershof.de

Received 16 January 2011; revision received 14 March 2011
Kvantovaya Elektronika **41** (4) 284–301 (2011)
Translated by V.L. Derbov

The progress of micro- and nanosystem instrumentation and sensor technologies results in fabrication and implementation of microanalytical systems that allow proceeding to a new level of miniaturisation of equipment and precision of measurements. Among the important reasons for that is the possibility to combine the sampling and probing functions in a single device.

In the present review we discuss the basic physical factors that cause the specificity of interaction of radiation with micro- and nanostructures, namely, with photonic crystal fibres (PCFs). Such structures not only provide a high degree of localisation of electromagnetic radiation due to the high gradient of the refractive index profile, but also allow higher efficiency of nonlinear optical processes [1]. All this offers new possibilities for solving the problems of biophotonics concerning both the miniaturisation and sensitivity improvement of biosensor devices and the essential extension of the field of biomedical application of laser technologies.

2. Types and classes of photonic crystal fibres

The concept of a photonic crystal (PC) [1, 2] was introduced in the 1980s. The structure of a photonic crystal possesses spatial modulation of the refractive index with the period comparable with the wavelength of the interacting radiation. With respect to the character of the refractive index variation, photonic crystals may be divided into three basic classes, namely, one-, two- and three-dimensional PCs. In one-dimensional crystals the refractive index periodically varies in one spatial direction. Such photonic crystals consist of parallel layers of different materials with different refractive indices and can manifest their properties in the only direction, perpendicular to the layers. Bragg structures, i.e., periodical structures of dielectric layers having the thickness $\lambda/4$ and two alternating values of the refractive index are an example of one-dimensional photonic crystals. Two-dimensional photonic crystals have the refractive index that periodically changes in two spatial directions, and they can also manifest their properties in two spatial directions. In three-dimensional photonic crystals the refractive index periodically changes in three spatial directions, and hence they are able to exhibit their properties in three coordinates; they can be represented as arrays of spatial bodies (spheres, cubes, etc.), arranged in a 3D crystal lattice.

Similar to electric media, photonic crystals can be divided into conductors, i.e., the substances that can transmit light along paths of large length with minor losses, dielectrics, i.e., next-to-perfect mirrors, semiconductors, i.e., the substances able, e.g., to reflect selectively the photons with a definite wavelength, and superconductors, in which due to collective

phenomena the photons can propagate along the paths of practically unlimited length [3].

We also distinguish between the resonance and non-resonance photonic crystals. The former differ from the latter by the use of materials whose dielectric constant (or refractive index) as a function of frequency possesses a pole at a certain resonance frequency.

Any inhomogeneity in a photonic crystal is called a defect of the photonic crystal, since it violates the periodicity. The region of the periodicity violation is, in fact, a microresonator, in which an electromagnetic wave is restricted in two dimensions, its intensity exponentially damping along the axis directed into the crystal. The wavelength of the fundamental radiation mode, concentrated in the defect of the structure, can be varied within the bandgap width by changing the size or shape of the defect [4].

Periodic structures with pronounced colouring often occur in nature [5–7]. Examples of one-dimensional periodic structures are the layers, coating the wings of some butterflies, the peacock tail feathers, the shells of some bugs. The role of interference in the colouring of the peacock feathers was noticed as far back as in 1730 by Isaac Newton. The structures with two-dimensional periodicity are present in the eyes of some insects, e.g., the moth, as well as humans and other mammalians, and also in some kinds of algae [8]. Two-dimensional periodicity is inherent in natural pearl, consisting of packed cylindrical elements.

The functionality of the living organism constitution, developed under the conditions of natural selection, suggests the special-purpose use of the optical properties of periodic structures in living nature. In many cases such purposiveness is obvious. The regular porous structure of the eyes of insects is an efficient antireflecting interface, providing the transmission of light and, simultaneously, the possibility of physicochemical metabolism between the inner eye tissues and the surrounding medium [7, 9]. The regular fibrillar structure of the eye cornea in humans and mammalians is also a photonic crystal with the property of interferential suppression of all scattered waves in the transverse direction and amplification of waves in the longitudinal direction [10]. Recently it was suggested that the periodic structure of diatoms promotes more efficient light collection, thus increasing the photosynthesis productivity [11]. The utility of interference coatings has no unambiguous interpretation yet. One may suppose that as a mechanism of colouring of living organisms the interference is preferable in comparison with the absorption because the interference colouring does not involve absorption and dissipation of the light energy and, therefore, is not accompanied with heating and photochemical destruction of the pigment coating.

Three-dimensional periodic structures occur in nature in the form of colloid crystals [12]. They were first observed in the studies of viruses [13]. The semiprecious stone opal is a colloid crystal, consisting of monodisperse spherical globules of silicon oxide [14]. It is just the light interference in the three-dimensional periodic structure that determines its sparkling colour, depending on the angles of incidence and observation.

A point defect in a photonic crystal, in fact, creates a waveguide. Based on this principle of trapping of electromagnetic radiation by the point defect, the conductors of optical radiation were designed which are referred to as photonic crystal waveguides [15]. The term 'photonic crystal fibres,' introduced by P. Russell in 1995 [15, 16], is a collective name for optical waveguides with a complex structured cladding, whose cross section represents a two-dimensional photonic crystal. An optical waveguide with the structured cladding, representing the geometry of a one-dimensional photonic crystal, is referred to as a Bragg waveguide [17]. The idea of designing optical fibres with a periodic cladding was formulated in 1978 [17]. Its novelty was to form a multilayer cladding, whose concentric layers have alternating (high/low) refractive indices. In such a structure the radial photon bandgaps appear that give rise to new guiding properties of the fibre. Note, that although the first publications on this issue are dated 1978, actually the work in this field began not long ago, in 1999–2000 [18, 19].

In such fibres a new method of controlling the structure-dependent refractive index of the cladding is implemented. As the refractive index of the fibre cladding decreases, the law of total internal reflection comes into effect, forming the base of the mechanism for trapping the electromagnetic radiation inside the fibre. The fibres of this type belong to the class of PCFs with solid core (Fig. 1a).

The second large class of PCFs are the hollow-core fibres (Fig. 1b, c). In these fibres the localisation of the optical radiation inside the core due to the total internal reflection is impossible. The guiding properties of a hollow-core PCF are due to the presence of a bandgap in the periodic structure of the cladding. The mechanism of reflection from the boundary between the core and the cladding is based on the Bragg reflection form a two-dimensional periodic dielectric structure [20]. The optical radiation with resonance frequencies lying within the crystal bandgap does not penetrate through the structured cladding of the fibre and propagates along the hollow core [21].

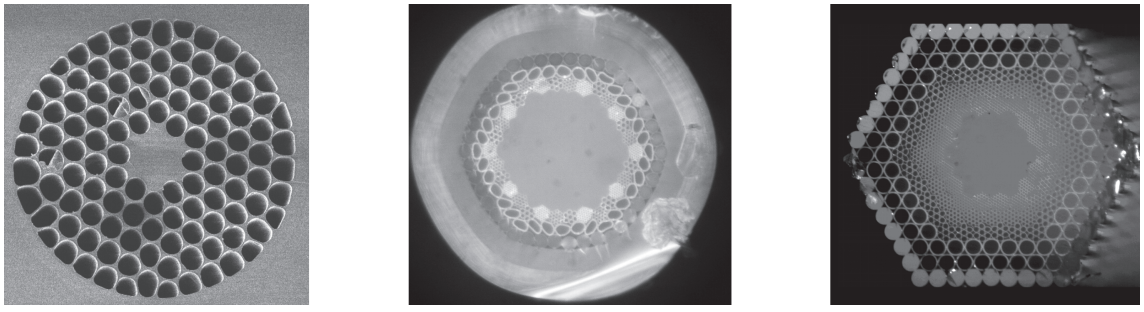

a b c

Figure 1. Photonic crystal waveguides (PCFs) with the solid (a) and hollow (b, c) core.

3. Technology of manufacturing photonic crystal fibres

Photonic crystal fibres were first made in 1995 [15, 17] of quartz capillaries stacked into a dense package and subjected to drawing. As a result the fibre was obtained with regularly distributed holes having the characteristic size ~1 μm. In PCFs the structured cladding is the region with longitudinal air-filled channels, packed into a hexagonal of square lattice, surrounding the core (solid or hollow), in which electromagnetic radiation is localised. The holes of the lattice may be of circular or arbitrary shape. The variation in the lattice type and spacing, the shape of air channels and the glass refractive index allows the properties that do not exist in usual fibres [22–26].

Photonic crystal fibres made of soft glass were first designed and fabricated by our research group in 2000 [27, 28]. They consist of regularly stacked capillaries or rods. The shape of individual elements, forming the fibres, and the topology of their stacking depend on the purpose of the manufactured article. The geometric parameters both of individual elements and of the whole structure may be arbitrary. In PCFs various types of glasses, differing in optical, electrical and chemical properties, may be combined. Combinations of glass with metal or graphite are also possible. All these combinations are designed based on the main requirement of matching the thermal properties of the elements (in particular, the thermal expansion coefficient).

The PCF fabrication is based on the following technological processes: drawing glassware from softened glass and redrawing the glassware [29]. Drawing is the most established classical technology of fabricating glassware in the form of tubes and rods of different shape and with different size of cross-section. In principle, the technology is the following. A block of glass wrapped in a heat-resistant cloth is placed on the filament extrusion device inside the furnace. When the block is heated up to the softening temperature, the softened glass, forced through the die hole by its own weight, moves down, where it is gripped by the drawing unit. Thus a rod or a tube is drawn. The shape of the cross section of the glassware and its size are determined by the geometry of the die hole, the drawing speed and the temperature of the softened glass. The stability and precision of keeping the furnace temperature constant and the rotational velocity of the drive of the drawing unit are largely responsible for the stability and precision of the geometric dimensions of the glassware cross section.

Besides the drawing from melt, the PCF fabrication technology includes the redrawing of the preform (tube, rod, package of tubes or rods) in similarity. Mathematically the procedure is described as

$$D_0^2 V = d_0^2 v,$$

where D_0 is the initial size of the preform (diameter, diagonal length of a hexagonal package or its size along double apothem); V is the speed of delivery into the furnace; v is the speed of drawing; and d_0 is the resulting size of the element.

The multistage technology of manufacturing the multichannel preforms consisting of many individual capillaries improves the regularity of stacking and allows producing the glassware of arbitrary size and with arbitrary channel diameters. The diameter of an individual channel may be as small as 50 nm. Due to different speeds of delivery and drawing the product acquires the cross-section pattern similar to that of the initial preform, but of smaller geometric size.

Thus, the shape of the glassware is determined by the shape of the preform, while its geometric size depends on the delivery-to-drawing speed ratio. To fabricate multichannel structures the elements are sorted out and stacked into a package, e.g., of hexagonal shape. The bundle is then heated up to the glass softening point, pulled-off with pincers and gripped by the feed motion that delivers it into the furnace. Being heated up to the softening point, the package is pulled-off with pincers and gripped in the drawing unit.

The desirable factor of cross-section size reduction with respect to the cross-section size of the preform, referred as redrawing coefficient, is provided by choosing the proper delivery-to-drawing speed ratio of the appropriate drives.

The stability and precision of the motion parameters of the drives largely determine the stability and precision of the geometric size of the cross sections of the product structures. For this reason high precision electric drives are used for the redrawing. Schematic diagrams of the fibre manufacturing and the drawing setup are shown in Fig. 2. Finally, the PCFs may have the following dimensions: the outer diameter 0.1–30.0 mm, the length 1200 mm, the diameter of inner channels 0.07–400 μm, the error in geometrical dimensions of the product ±(0.5–1.0)%.

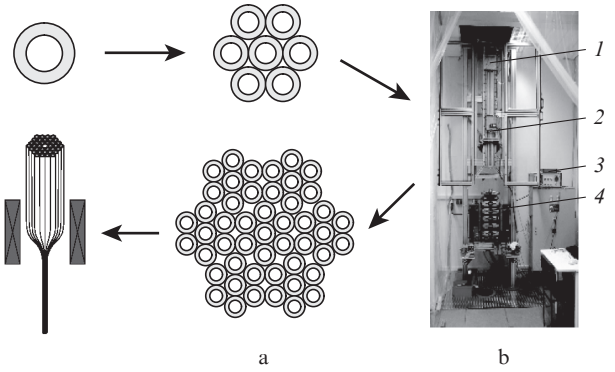

Figure 2. Schematic diagram of PCF manufacturing (a) and the setup for PCF drawing (b):
(*1*) mechanism for the delivery of glass elements into the furnace; (*2*) furnace; (*3*) control unit for delivery and drawing parameters; (*4*) chain drawing mechanism [29].

4. Optical properties of the photonic crystal fibres

The scope of the PCF properties [30–34] is very wide and many aspects related to the physics of these structures still remain unexplored.

The waveguide performance of these PCF is implemented via the internal reflection from the periodic structure and the appearance of a wide bandgap for the radiation, propagating along the axis of the waveguide. The photonic bandgaps and the dispersion for different wavelengths may be tuned by changing the structure geometry only. It is not necessary to use other dielectric materials.

In a wide spectral range only the modes of the lowest (zero) order propagate along the waveguiding defect of the photonic bandgap structure, while the higher-order modes exit

into the cladding and decay. This phenomenon was called modified effect of total internal reflection, when the band structure of the photonic crystal manifests itself only implicitly, and its waveguide properties for the zero-order modes are determined by the total internal reflection. The number of guided modes in the defect is determined only by the ratio of the diameter d of the air channels and the separation Λ between their axes. In the case when $d/\Lambda \leqslant 0.2$ the PCF is single-mode in the whole spectral range of quartz transparency [35].

In this situation (Fig. 1) no perfect periodicity of hollow channels in the cladding is required, since the crucial factor is the value of the mean refractive index of the cladding. The presence of the hollow channels allows the difference between the refractive indices of the waveguide defect and the cladding be enlarged by more than an order of magnitude as compared with the standard fibre. This fact mainly determines the principal novelty of the PCF properties.

Besides the mentioned possibility of designing a single-mode PCF in a very wide spectral range, the PCF dispersion properties that depend on the size and relative location of the air channels are also unusual. Photonic crystal fibres can possess anomalous dispersion of the group velocities in much shorter-wavelength spectral region, than the usual fibres. The absolute value of the dispersion in holey fibres may be an order of magnitude larger that in standard single-mode fibres and the dependence of the dispersion upon the wavelength may be very weak in a wide spectral range.

However, changing all the geometric sizes of the waveguide structure (provided that the proportion between them is conserved), one can achieve single-mode operation of the waveguide with both the small and the large effective cross-section area of the mode [35], which is of primary importance for practical applications. The large size of the core allows reducing the effect of nonlinear phenomena on the light pulses, propagating through the fibre, and vice versa, at small mode field size the role of nonlinear effects may be essentially greater than in standard fibres.

To describe the mode propagation in PCFs with solid core and triangle stacking of the cladding the method was proposed [35] to estimate the transparency of the structured cladding using the period and diameter of air capillaries, based on the calculation of the effective refractive index, well-known in common waveguides. The results of the calculation are then applied to a common fibre model, comprising the core with the refractive index of pure quartz $n_c = 1.45$ and the cladding with the calculated effective refraction index n_{cl} of the structured domain.

The first approximation of the method of effective refraction index n_{eff} consists in the determination of the field Ψ of cladding modes, which results from the solution of the scalar wave equation within the simple centered cell, comprising a single hole. The diameter of the cell is equal to Λ, i.e., the separation between the axes of the holes.

Using the mirror symmetry properties, the boundary conditions at the cell perimeter are formulated as $d\Psi/ds = 0$, where s is the normal to the boundary, i.e. at the angle points of the cell the constant field is equal to that on a circular boundary of the cell. The propagation constant of the fundamental mode β_{fm} is found from the equation $n_{eff} = \beta_{fm}/k$, where k is the wave vector.

Significant interest is attracted by the ability of photonic crystal fibres to demonstrate nontrivial laws of refraction that change depending on the frequency of the incident light. In particular, from the practical and scientific point of view an important manifestation of unusual dispersion in periodic media, or photonic crystals, is presented by the negative refraction [36, 37], i.e., the refraction in which the group velocity vector of the refracted wave forms an acute angle with the tangential component of the wave vector of the incident wave. The refraction of such kind is typical for so-called left-hand media, or media with negative permittivity and permeability. A photonic crystal is able to demonstrate negative refraction, possessing positive effective values of both permittivity and permeability and having the period, comparable with the wavelength, at which the mentioned effects are observed. Negative refraction offers additional opportunities of manipulating with the refracted beams, which, alongside with the normal refraction, can be potentially used in complex light-controlling systems.

It is known that the spectral characteristics of PCF depend on the configuration of the structured cladding, because the structural properties together with the presence of the central defect in the lattice are the conditions for the formation of a photonic bandgap. One can vary the spectral composition of the radiation output from the waveguide by changing the parameters of the structured cladding, namely, the number and position of channels and their diameter.

The change of at least one of the geometric parameters of the structured cladding causes the transformation of the spectrum of radiation, transmitted by the waveguide. Figure 3 presents the spectra of radiation transmitted through the PCF samples with the same number and stacking of channels in the structured cladding. The difference between the samples consists only in the channel diameters. From the analysis of the presented spectra it is seen that in the first waveguide (Fig. 3a) the structured cladding possesses high reflectance in the wavelength intervals 400–500 nm and 740–820 nm. The guided modes in these intervals essentially contribute to the registered signal. In the interval of wavelengths 500–740 nm the optical radiation is unable to propagate in the waveguide. The second waveguide (Fig. 3b) has the transmission band in the interval 600–800 nm.

Nonlinear effects in PCFs [38] are very interesting and much less explored. When an intense laser radiation propagates through a medium, the induced polarisation arises in it

$$P = \varepsilon_0(\chi^{(1)}\bar{E} + \chi^{(2)}\overline{EE} + \chi^{(3)}\overline{EEE} + ...),$$

where ε_0 is the dielectric constant of vacuum; $\chi^{(j)}$ is the susceptibility of the jth order; $\bar{E}$ is the electric field. For any three-wave process $\chi^{(2)}$ is equal to zero, because the medium possesses inversion symmetry, and $\chi^{(3)}$ becomes the most significant nonlinear component. This component is responsible for such processes as phase self-modulation, phase cross-modulation, third harmonic generation, four-wave mixing, Raman and Brillouin scattering.

In [20] it was proposed to introduce a nonlinear material into the channels of the periodic structure, and in [39] the implementation of such structure was reported. The manufactured waveguide with the core diameter 1.7 μm had the coefficient γ of nonlinear transformation 25 times greater than in common optical fibres. Let us briefly consider the origin of such a great nonlinear transformation coefficient. Assume that a PCF has air channels filled with an efficient nonlinear medium, with the linear refractive index n_0, exceeding that of the glass matrix, and with positive nonlinear refractive index n_2. Under applying an intense signal I_p the difference between the refractive indices of the matrix and the medium will be

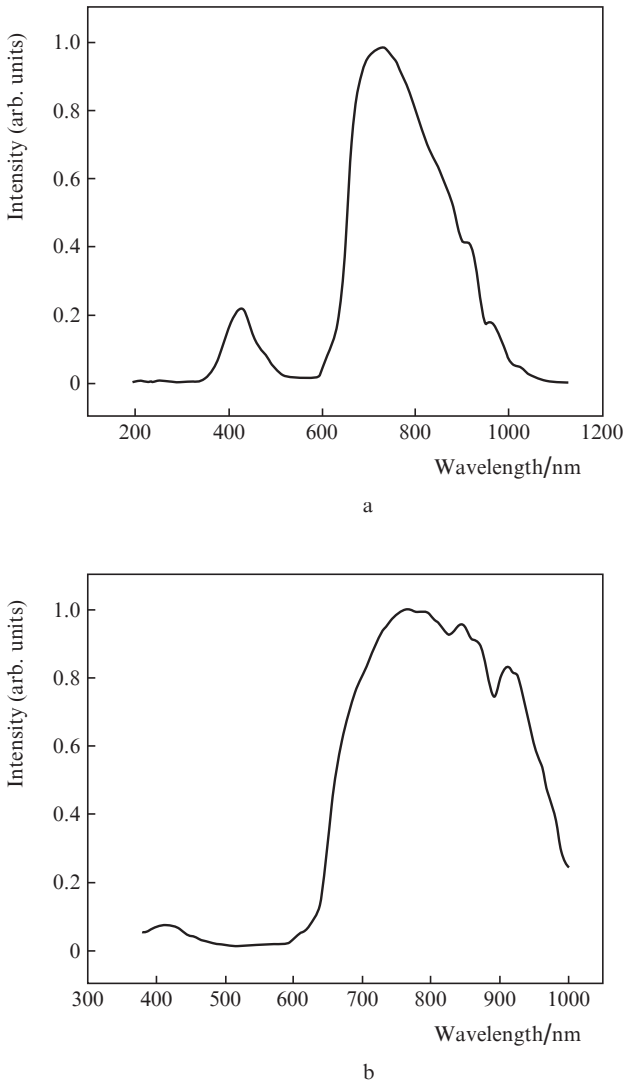

Figure 3. Spectral characteristics of PCFs with the diameters of hollow core 113 μm (a) and 89 μm (b), diameters of a single channel 2.6 μm (a) and 2.1 μm (b), the wall thickness near the hollow core 240 nm (a) and 180 nm (b) [32–34].

increased, $n_{cl} = n_0 + n_2 I_p$. According to the calculations of [40], the increase in the difference between the refractive indices leads to the increase in the bandgap width.

From the issues, considered above, it follows that since at the edge of the bandgap the light propagation velocity tends to infinity, the PCF simulates a medium with the effective dielectric constant, close to zero [41]. Far from the bandgap the effective permittivity is determined by the mean permittivity of a unit cell of the structure. Within the bandgap the effective permittivity must be negative, since the electric field is damped in the structure and, therefore, at the edge of the bandgap a transition zone is expected to exist, where the permittivity vanishes. As shown by calculations and experiments [42, 43], a light beam (incident on such a layer) with the wavelength corresponding to the thickness of the transition zone experiences large-angle refraction in the direction, opposite to that occurring in classical materials with the permittivity greater than 1. This phenomenon is called 'superprism' and may be used to design ultra-miniature high-resolution single-chip spectrometers [43].

The authors of [44, 45] report the propagation of a megawatt-power laser pulse in a hollow-core PCF, which is practically impossible in common fibres because of frequency conversion caused by the Raman scattering and phase self-modulation. From the practical point of view, the transmission of high-power pulses may be used in the solution of many problems of technology and biomedicine [46].

One of important applications of nonlinear optics is the generation of supercontinuum, i.e., the coherent electromagnetic radiation with a superbroad spectrum. The generation of supercontinuum, first observed in the glass sample using a mode-locked laser [47], was also demonstrated in water [48] and gas flow [49]. The appearance of femtosecond lasers operating at the wavelengths 1.3 and 1.5 μm allowed supercontinuum generation in common optical fibres. The parameters of the supercontinuum are significantly improved, if the wavelength of the pump pulses falls within the wavelength region of zero group velocity dispersion of the waveguide. In this case nonlinear effects in the fibre predominate over the dispersion ones [50], which makes it possible to reduce the length of the fibre from kilometres to a few tens of metres. In this case wide application was acquired by the waveguides, comprising the materials with a high nonlinearity coefficient in their structure, as well as by the fibres with a special dispersion profile, varying along the fibre length [51]. Their use allowed the generation of supercontinuum more than 300 nm wide.

In PCFs the supercontinuum generation was first demonstrated in [25]. In the experiments [25, 26] the 100-fs pulses from a 800-nm Ti : sapphire laser were used. The pulses were introduced into a 75-cm-long PCF, the output radiation had a continuous spectrum in the region 400–1600 nm.

In the experiments [52] they used a Ti : sapphire laser (70 fs, 850 nm, 300 mW) and a tapered (conical) Corning SMF-28 fibre. The supercontinuum spectrum width was greater than two octaves (370–1550 nm).

The first results of the study and modelling of supercontinuum generation in PCFs were presented in the papers [53–55], from which it followed that the supercontinuum generation is affected by soliton effects. The confirmation was obtained in 2010 [56]. When ultrashort light pulses are sent through a PCF for producing supercontinuum, the spectrum broadening over the whole visible and near IR ranges gives rise to solitons, i.e., nonlinear solitary waves that conserve their shape and velocity in the course of their own motion and collisions with similar waves. The only result of the interaction between solitons may be a phase shift [57, 58]. The solitons block the light pulses that follow them, making them to reduce their wavelength and to shift to the blue, while the solitons themselves shift towards longer wavelengths (to the red). This double effect leads to the broadening of the spectrum. As a result, the radiation with ultrawide frequency spectrum, which is a characteristic feature of supercontinuum, is generated at the output of the fibre.

Generation of supercontinuum in a PCF with a periodically structured cladding was first reported by us in 2003 [59]. The use of a two-dimensional periodic photonic crystal lattice allowed strong localisation of radiation in the defect without using the effect of photonic bandgaps. In this case, due to total internal reflection, the radiation propagates along the defect, generated by the structure crossing point of the so-called kagome lattice.

The PCF (Fig. 4) was made of electron-tube C-52-2 glass and had the following parameters: the outer diameter of the structure 212.98 μm, the defect diameter 4 μm, the outer diam-

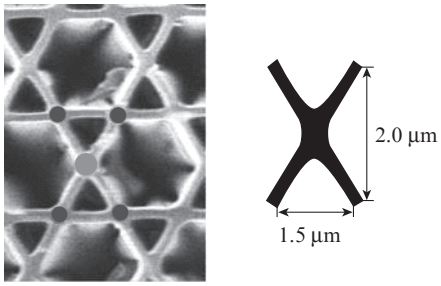

Figure 4. PCF with a periodically structured cladding of the kagome type (local dimensions 2.0 μm×1.5 μm) for supercontinuum generation.

eter of defect 12.54 μm, the diameter of small holes 2.62 μm, the period of holes in the defect 4.23 μm, the diameter of surrounding holes 8.09 μm, the structure period 11.09 μm, the area of intermediate triangles 4.41 μm^2, the optical transmission of the structure 69.4%. The nonlinear refractive index of the waveguide glass was $n_2 = 4.5\times10^{-16}$ cm^2 W^{-1}, which corresponds to the nonlinearity coefficient of the glass $\gamma = 0.15$ W^{-1} m^{-1} [59].

The experimental setup for supercontinuum generation [59] is shown in Fig. 5. The radiation from the Ti:sapphire laser (*1*) after the rotary mirrors (*2*) was incident on the beamsplitter (*3*) and split into two beams. The beam passed through the microscope objective (*4*) (magnification 65×, focus length 2.67 mm, numerical aperture NA = 0.85) and the PCF segment (*5*). The ends of the PCF were fastened to the three-coordinated table with micrometer feed motion. After passing the PCF the radiation passed through the lens (*6*) ($f = 8$ mm) and entered the CCD-camera with the beam analyser (*7*). The rotary mirror (*2*) placed between the lens and the camera could direct the radiation either into the spectrometer (*9*) (wavelength range 350–1800 nm) with the matching lens (*8*) ($f = 150$ mm), or into the UV spectrometer (*12*) (wavelength range 180–340 nm) with the lens (*11*) ($f = 80$ mm). In the other arm of the setup the laser radiation was sent directly into the spectrometer (*10*).

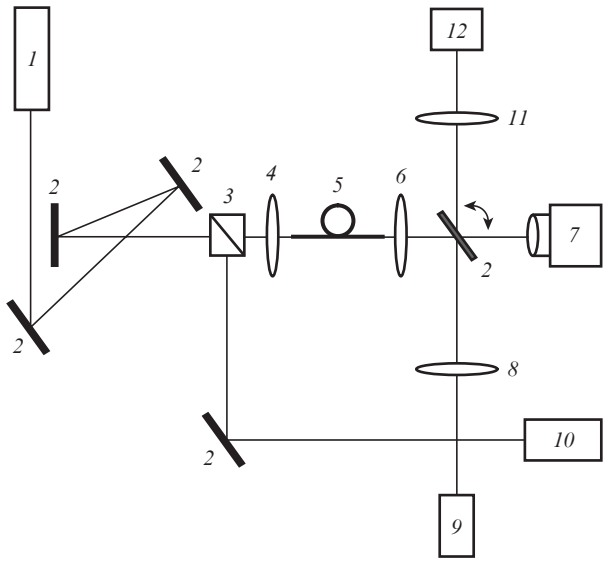

Figure 5. Schematic diagram of the experimental setup for supercontinuum generation:
(*1*) Ti:sapphire laser; (*2*) rotary mirrors, (*3*) beamsplitter; (*4*) microscope objective; (*5*) PCF; (*6*, *8*, *11*) lenses; (*7*) CCD-camera; (*9*, *10*) spectrometers (350–1800 nm); (*12*) UV spectrometer (180–340 nm).

The Tsunami 3941-MIBB mode-locked Ti:sapphire laser (Spectra Physics) was used as a source of intense ultrashort pulses. It comprised the cavity with the acoustic modulator and the active feedback for generating ultrashort pulses [60]. The dispersion compensation in the laser cavity was implemented using a prism. The laser generated pulses of Gaussian shape with the duration ~100 fs and the repetition rate 80 MHz. The laser wavelength was tunable from 700 to 900 nm, the radiation bandwidth in the pulsed regime was ~15 nm with the mean power of 900 mW at the wavelength 800 nm. The $1/e^2$ diameter of the beam was less than 2 mm. In the course of the experiment the laser radiated at $\lambda = 790$ nm, the pulse duration being ~220 fs.

The laser radiation was focused with a microscope objective exactly onto the crossing of the structured lattice, i.e., onto the kagome-type PCF defect (Fig. 4). Then the laser power was increased until the waveguide started to generate supercontinuum. Using such a structure (the defect size 1.41 μm, the sample length 30 cm) the supercontinuum radiation was obtained, measured with the spectrometer having the band 350–1800 nm (Fig. 6b). The registered spectrum occupied the whole spectrometer operation band (1450 nm), and the additional measurements of the broadening using the UV spectrometer (Fig. 6a) have shown that the total width of the spectral contour was 1620 nm.

One can see from Fig. 6c that the supercontinuum generation using the defect of the PCF with a kagome lattice is possible under the excitation with the same laser providing nearly the same power density (~40 GW cm^2) in the fibre samples of different length up to 1.5 cm.

An important factor, affecting the supercontinuum generation, is the input power of the pumping radiation, which in our case was 660 mW, providing the power output from the fibre about 6 mW.

The structure, designed by us, with the 1.41-μm defect, surrounded by holes with the diameter, smaller than that of the holes of the main matrix, allowed the shift of the lower supercontinuum boundary to 180 nm. In [61] the spectral broadening to somewhat wider range (350–2200 nm) is reported with the excitation of the fibre at larger wavelength (1.55 μm) and the defect diameter 2.6 μm. Recently [62] the supercontinuum generation was reported in the IR region of 700–250 nm under the excitation of a solid-core PCF, made of lead–bismuth–gallium glass. The pump from an optical parametric oscillator (1540 nm, 120 fs) provided high uniformity of the spectrum (at the level of 5 dB) in the range 1000–2500 nm.

In 2008 the PCFs with chirped cladding (CPCF) were first designed and investigated [63]. Chirped photonic crystal fibres are hollow-core waveguides whose structured cladding is formed by layers of holes, arranged in correspondence with a certain law (Fig. 7a). The radiation with different wavelengths is reflected from different layers of the photonic crystal structure (Fig. 7b).

To prove the efficiency of the chirped waveguide operation, the laser pulse with the duration 13 fs and the energy 4.3 nJ was introduced into the PCF hollow core (Fig. 8a). The sample length was 1 m and the diameter of the hollow core was 53 μm. The duration of the output pulse was 26 fs (Fig. 8b), the transmission coefficient being equal to 21%. For comparison, in a standard commercial PCF with the hollow-core diameter 9.5 μm a similar input pulse is broadened to 3.5 ps at the transmission coefficient of 47%. Therefore, CPCFs offer new facilities for

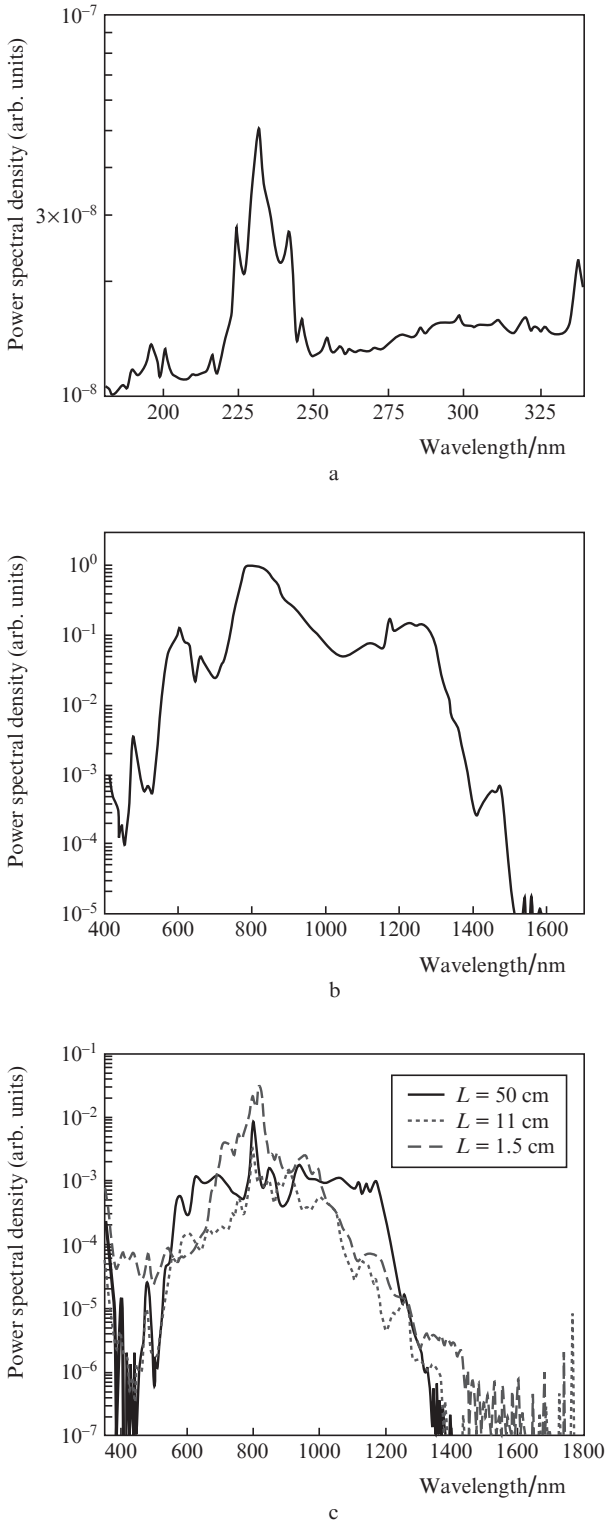

Figure 6. Supercontinuum generation using the kagome-lattice PCF: the UV part of the supercontinuum spectrum (a), the visible and IR parts of the supercontinuum (b) and the spectra, excited in the PCF by the radiation of the femtosecond Ti : sapphire laser (~800 nm, ~220 fs) at nearly the same power density (~40 GW cm^{-2}) in the fibre and different fibre lengths (c) [59].

transporting femtosecond radiation over the distances, sufficiently long for many applications in biophotonics, with minimal losses and distortions of the pulse shape [63, 64].

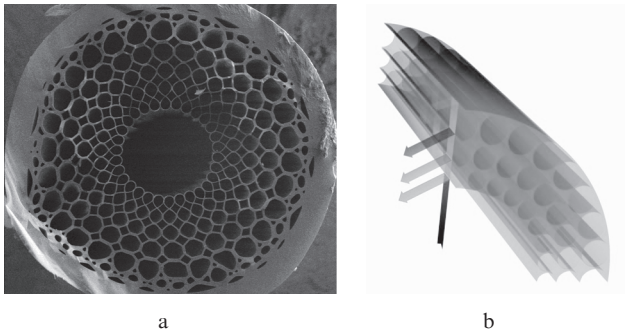

Figure 7. Cross section of a waveguide with chirped cladding (a) and the scheme of reflection from the waveguide chirped cladding (b).

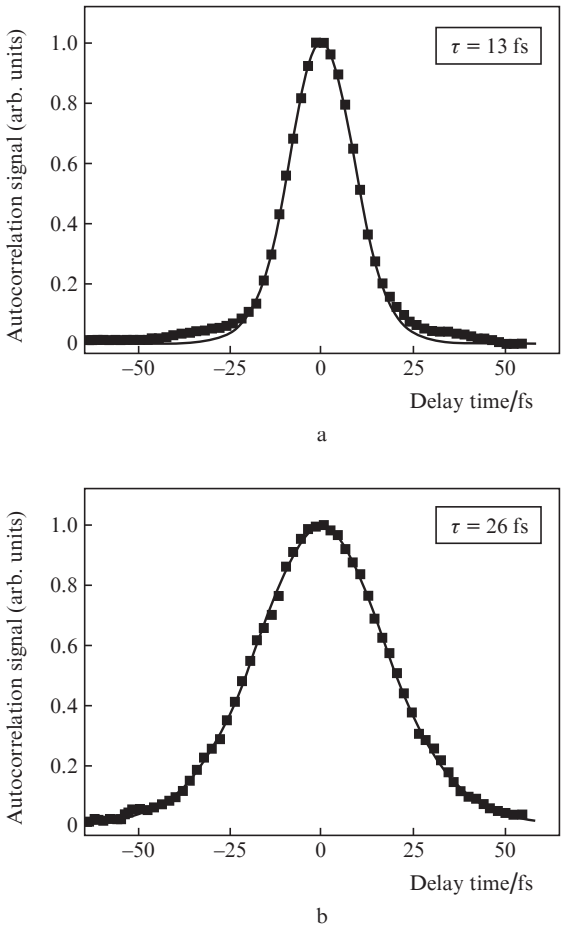

Figure 8. Profiles of a femtosecond laser pulse at the input (a) and output (b) of the chirped PCF.

Supercontinuum generation in PCFs can have multiple applications, e.g., as a broadband (low-coherence) source for biological tissue imaging [65], for wavelength multiplexing in communication systems, in systems of precise frequency metrology [66–71]. In telecommunication high-density wavelength multiplexing systems [72] a single supercontinuum source may be used instead of multiple sources for spectral channels, providing the generation of more than 1000 channels [73–75], which will surely also find application in biophotonics in the nearest future.

The stimulated Raman scattering in PCFs was first used for optical amplification in [76]. In the experiment the laser

radiation with the wavelength 1536 nm was introduced into the 75-m-long PCF. At the output of the fibre the power gain was 42 dB.

The development of new types of PCFs opens a new stage in the progress of optical technologies for biomedicine, allowing drastic enhancement of all basic nonlinear optical processes and offering the possibility of supercontinuum generation using nano- and sub-nanojoule femtosecond pulses. The supercontinuum generators on the base of micro- and nanolightguides help to provide extreme precision of optical measurements and open the ways for designing new compact multiplex radiation sources for nonlinear spectroscopy and microscopy, laser therapy and cell nanosurgery [77–79].

5. Biological sensors based on photonic crystal fibres

Biosensors are a new class of analytic devices, in which the immobilised biological materials are used for the recognition of molecules. The idea of creating a biosensor device was first stated about 30 years ago [80]. This idea was to use an enzyme electrode, i.e., an electrochemical sensor with an enzyme immobilised over its surface. During the passed decades numerous studies were carried out in relation to different aspects of protein electrochemistry on the electrode surface, which made it possible to create a number of biosensors on the base of enzyme electrodes, some of them already implemented commercially. Depending on the specific biological sensitivity of the element, the biosensors are divided into enzyme, immunological and microbe ones, and depending on the detector type into electrochemical, optoelectronic, acoustic and optical ones.

Optical biosensors possess high sensitivity and resolution in the detection and quantitative assessment of chemical substances and biological processes [16, 81]. Depending on the type of the optical sensors, their action is based on different optical phenomena, including absorption and reflection of the incident flux of light, luminescence, surface plasmon resonance, and the effect of photonic bandgaps. The signal of an optical biosensor can be described in terms of the variation of the wavelength, intensity, phase and polarisation of light depending on the concentration of the detected substances and the influence of the environment. Typically a biosensor includes a light source, a unit introducing the radiation into the sensor, and a device for analysing the radiation spectrum, mode profile, etc. [16, 82].

Many optical fibre biosensors are designed to make use of the exponentially decaying (evanescent) waves, localised in the cladding of the fibre [16, 83]. The light guide consists of a high-index cylindrical core and a low-index cladding. The radiation propagates in the core of the fibre due to total internal reflection. In the cladding the penetration depth of the evanescent field is of the order of the wavelength and depends on the mode refractive indices and the cladding material. By partially removing the cladding material one can provide direct interaction of the evanescent field with the biological analyte, which allows plotting the evanescent field intensity versus the analyte refractive index [16, 83].

Biosensors based on the surface plasmon resonance are one more class of optical sensors that allow real-time analyte detection without using fluorescent probes [84–86]. The plasmon resonance, i.e., the surface excitation of plasmons by light, occurs at the surface of metals under the conditions of total internal reflection and is characterised by certain refractive index and reflection angle. The measurements are based on the migration of the plasmon resonance energy from the surface of the metallic film into the solution, where, due to the intermolecular interaction, the change in the resonance angle and, therefore, in the refractive index in the near-surface layer occurs. Basing on the change in the latter, one can judge about the interaction between the biological molecules. The variations in the refractive index are largely affected by the medium, surrounding the metallic nanostructure. The change in the refractive index is detected in the immediate vicinity of the nanostructure, owing to which the phenomenon of local plasmon resonance may be used for the label-free assay. The films are most frequently made of gold or silver. Other metals can be also used for the assay, provided that the frequency of the plasmon resonance overlaps with that of the protein optical absorption [87]. The sensitivity limit of such a sensor is 1 pg mm^{-1} [84].

At present PCFs are considered as one of the most promising sensitive elements of fibreoptical sensors of physicochemical quantities, the use of which would substantially improve the performance capabilities of traditional fibre biosensors. Their basic advantages include the electromagnetic noise immunity (as in many fibreoptical sensors), high sensitivity, reliability, reproducibility, wide dynamic range of measurements, the possibility of spectral and spatial multiplexing of sensitive elements, located in one or a few waveguides, short time of response to the variation in the measured quantity, small outer dimensions, the possibility to combine waveguide principles and microfluidistics.

The position of the optical radiation transmission regions and the photonic bandgap of a hollow PCF are largely affected by the refractive index of the medium, filling the space in the hollow core and the channels of the cladding. The sensitivity of the PCF spectral characteristics to the physical parameters of the medium (gas or liquid), filling its internal structure, determines the promising applications of the waveguides in the analytic devices (biological chips and sensors), used in biology and medicine. The possibility of using PCFs as sensors was first noticed in [88], where the absorption spectra were measured for acetylene that filled a waveguide under pressure. In [89] the possibility of designing a photonic crystal sensor was reported that allows detection of individual molecules via their two-photon fluorescence. The possibility of selective detection of antibodies in a hollow PCF was shown in [90].

Two protocols of implementing biological PCF-based sensors were demonstrated [91]. The first protocol is based on the waveguide with a double periodic structured cladding and core. The radiation from a diode laser (532 nm) is introduced into the core of the waveguide and is captured there due to the guiding properties of the first structured cladding. The radiation is transported to the probed sample and the excited fluorescence is collected by the second structured cladding. In the second protocol the biological sample, marked with a fluorescent dye, is introduced into the structured cladding of the waveguide. The laser radiation is focused into the core, and the radiation, passing through the waveguide, is studied. As shown in Ref. [91], these two protocols are completely identical with respect to the character of the acquired data about the biological analyte.

To design a new generation of biosensors one needs detailed investigations of the character and the degree of influence of the substances under study on the spectral properties of the PCF [92]. For example, we used aqueous solutions of

riboflavin and cyanocobalamin of different concentrations as the model of a liquid, strongly absorbing light in the visible region of wavelengths.

The aqueous solution of riboflavin (at large concentrations) is a liquid having intense yellow-orange colour. Riboflavin is a biologically active substance. Its molecule is formed by the ribose and the yellow pigment flavine (from Latin '*flavus*' meaning yellow). Riboflavin, excited at the wavelength 370 nm, is used, e.g., as a photodynamic photosensitiser for generating singlet oxygen and other superoxide free radicals that participate in the process of extracorporal photodynamic therapy of the whole blood and its individual components [93]. It is used also in the form of the Medio-Cross® preparation (the solution of riboflavin and dextran), owing to which the generated radicals provide the creation of physical bonds between collagen fibres in biological tissues (e.g., the eye cornea), necessary for mechanical strengthening of the tissues in the treatment of numerous diseases [94]. The derivatives of riboflavin, flavine mononucleotide (FMN) and flavine adenine dinucleotide (FAD) enter into the composition of many redox enzymes as coenzymes. Aqueous solutions of riboflavin have two broad absorption bands at 370 nm and at 445 nm.

To explore the mechanisms responsible for the change in the PCF spectral properties depending on the concentration of riboflavin solution, introduced into the channels, we used the chirped-cladding waveguide, consisting of five concentric layers (Fig. 7a) with the diameter of the hollow core 284 μm and the outer diameter 1 mm.

Figure 9 presents the spectrum of radiation, passed through the PCF sample with the abovementioned parameters and with the channels filled with air. The spectrum has a comb-like structure, and eight intensity peaks with a large modulation depth appear in the sensitivity interval of the spectrometer. For further analysis of solutions one should first obtain the reference signal, i.e., the transmission spectrum of the PCF with its channels filled with pure solvent. In the present case this solvent was water. Figure 10 presents the spectrum of radiation, passed through the 50-mm-long PCF with its channels filled with distilled and deionised water. Now only six intensity maxima are present in the spectrum, not eight, as in the case of filling with air. The spectrum transformation is due to the significant change in the refractive index of the

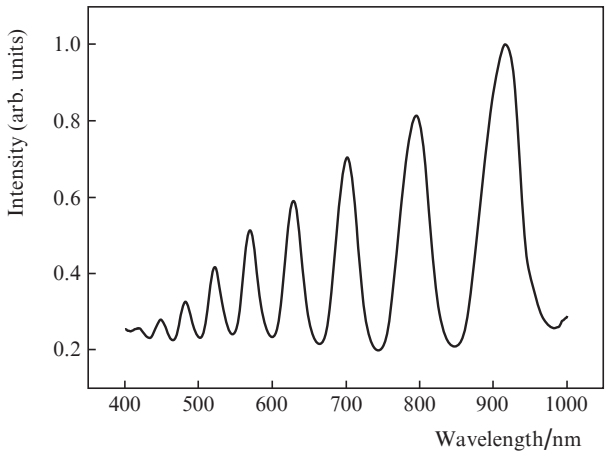

Figure 9. Spectrum of optical radiation, passed through the PCF sample with chirped cladding.

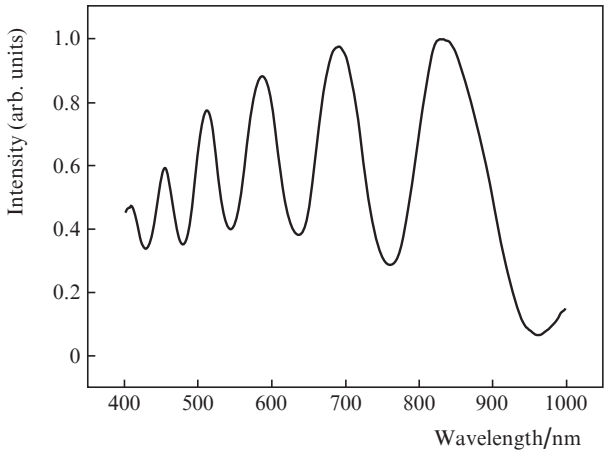

Figure 10. Spectrum of radiation, passed through the PCF sample, filled with water (n = 1.33).

medium in the hollow channels of the fibre. The presence of the intensity maximum at 450 nm in the spectrum is of primary importance, because its position exactly coincides with that of the intrinsic absorption maximum of riboflavin. It is reasonable to expect that the amplitude of this peak will be most sensitive to the variations in the solution concentration.

Five solutions with the riboflavin concentrations 0 (water), 0.001, 0.003, 0.005, and 0.01 mg mL^{-1} were used in the experiment. The transmission spectra are presented in Fig. 11. It is seen that with the growth of concentration the transmission spectrum of the filled PCF is apparently transformed. Significant reduction (up to suppression) of the intensity maximum at 450 nm occurs, as well as considerable lowering of the neighbouring maximum ($\lambda \approx 520$ nm). Using these spectra we plotted (Fig. 12) the peak amplitude at λ = 450 nm versus the concentration of the solution. The height of the peak at λ = 450 nm decreases exponentially with the growth of the solution concentration, which is well confirmed by the proper

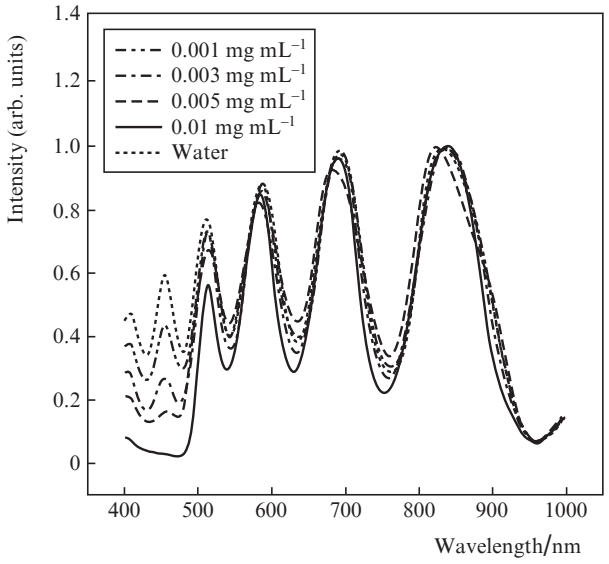

Figure 11. Spectra of radiation, passed through the PCF samples after filling the channels with aqueous solution of riboflavin with different concentrations.

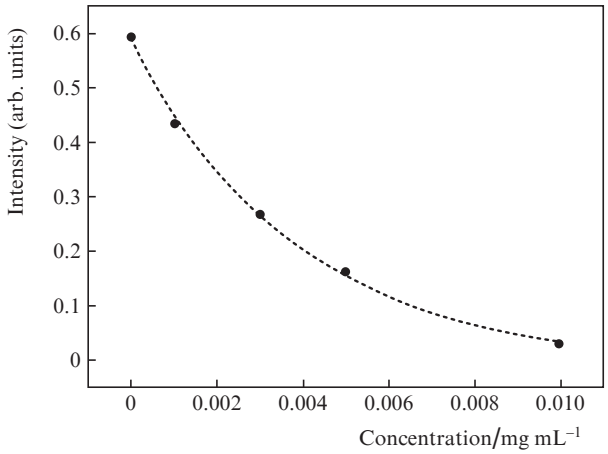

Figure 12. The peak amplitude at λ = 450 nm versus the concentration of riboflavin solution in PCF.

approximation. On the contrary, the intensity maxima (Fig. 11) in the longer-wavelength region of the spectrum are practically insensitive to the variations in the riboflavin concentration. This fact shows that it is the absorption at the wavelength 450 nm that affects the character of light propagation most strongly.

The studies carried out have shown that the use of a PCF for measuring the solution concentration allows the detection of the concentration change in the solution under study at the level $\sim 10^{-4}$ mg mL^{-1} (10^{-5}%) and the detection of a substance at concentrations $\sim 10^{-5}$ mg mL^{-1} (approximately 10^{-8} mol L^{-1}).

The change in the spectral characteristics of waveguides due to the change in the refraction index of the medium filling the PCF channels makes it possible to use the waveguides for measuring the refractive indices of liquids and gases. Thus, in Fig. 13 three transmission spectra of waveguides with channels filled with glucose solutions of different concentrations are shown. The glucose concentration affects the refractive index of the solution, namely, when the concentration changes from 1% to 40% the refractive index varies in the interval 1.3356–1.3919 (at 20 °C).

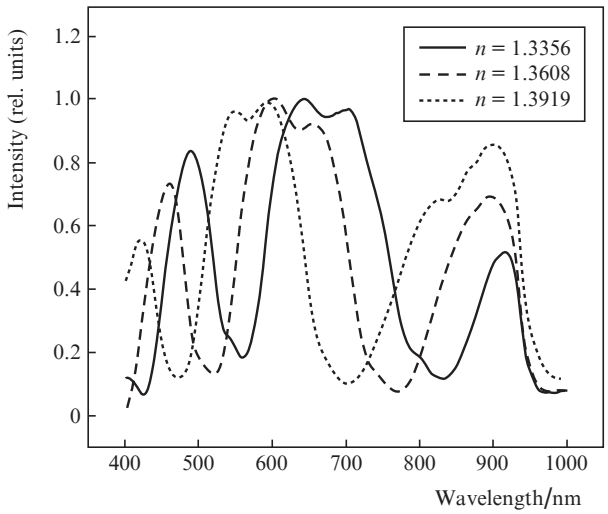

Figure 13. Spectra of radiation, passed through the PCF samples after filling the channels with aqueous solutions with different refractive indices.

The analysis of the spectra (Fig. 13) shows that with the increase in the medium refractive index the short-wavelength peak in the spectrum of the output radiation is shifted towards the long-wavelength region and grows in amplitude. On the contrary, the central maximum is shifted towards the shorter-wavelength region, and the adjacent shorter-wavelength maximum also increases in height. Such shifts of the peaks in the spectrum occur owing to the uniform growth of the refractive index at all wavelengths.

One more example of PCF application is the measurement of the cholerogenum concentration in aqueous medium (Fig. 14). The subject of study is the liquid, containing cholerogenum. The latter is a toxin of protein nature, produced by comma bacillus. It is fixed by the receptors of the cells of the small intestine mucosa and causes diarrhea in the cases of cholera. One can see from Fig. 14 that within the limits, necessary for monitoring the toxin in the laboratory conditions, the increase in the solution concentration considerably changes the spectrum of the light transmission.

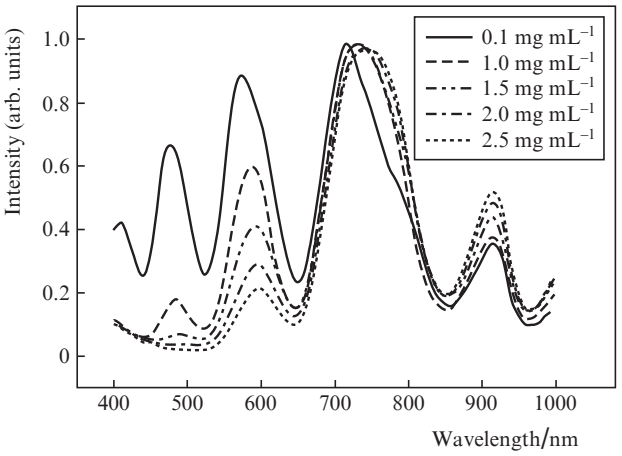

Figure 14. Spectra of radiation, passed through the PCF samples after filling the channels with aqueous solutions of cholerogenum with different concentrations.

It is important that even though the sensitivity to the changes in the refractive index of three studied solutions appeared relatively small and slightly lower than in the commercial refractometers, PCFs still demonstrate essential advantages over them. They include the possibility to acquire information at many wavelengths at once and information about the absorption of the studied substance, and also to automate the process by using disposable microcuvettes with built-in PCFs. Besides, the optimisation of the spectral data processing would increase the sensibility by at least an order of magnitude.

It should be noted that the high sensitivity of the intensity of radiation, passed through a waveguide, to the change in concentration of scatterers in the hollow core of the waveguide may provide the base for a new method of blood grouping in humans [95–97].

Table 1 gives a brief description of known biosensors and the data about their sensitivity [98].

Basing on the photonic crystals, an 'intelligent' Petri dish was designed [99]. The principle of its operation is the follow-

Table 1. Relative characteristics of biological sensors

Design concept	Optical method	Analyte	Sensitivity limits	References
Surface plasmon resonance	SPR	Solutions	10^{-5}–10^{-6} (RI)	[131–136]
	Broadband SPR	Solutions	10^{-7}–10^{-8} (RI)	[137, 138]
	SPR tomography	Solutions	10^{-5}–10^{-7} (RI)	[139–142]
	SPR tomography	Proteins	1 nmol	[143]
	Optical heterodyne SPR	Proteins	0.2 nmol	[144]
	Phase-sensitive SPR	Proteins	1.3 nmol	[145]
	Wavelength-modulated SPR	DNA	10 nmol	[146]
	SPR tomography	DNA and RNA	10 nmol	[147]
	Flow-injection SPR	DNA	54 fmol, 1.38 fmol	[148, 149]
	Angle-modulated SPR	Protein (PSA)	0.15 ng mL^{-1}	[150]
	SPR	Protein (CA19-9)	66.7 ml^{-1}	[151]
	SPR	Protein (α-fetoprotein)	50 ng mL^{-1}	[152]
	Prism-based SPR	Bacteria (*E. coli*)	106 CFU mL^{-1}	[153]
	Prism-based SPR	Bacteria (*Salmonella yphimurium*)	100 CFU mL^{-1}	[154]
	SRP BIAcore 2000	Bacteria	25 CFU mL^{-1}	[155]
Interferometry	Mach–Zender interferometer	Solutions	10^{-7} (RI)	[156]
		Proteins	20 pg mm^{-2}	[157]
	Young interferometer	Solutions	10^{-7} (RI)	[158, 159]
		Viruses	1000 particles mL^{-1}	[160]
	Hartman interferometer	DNA	4 ng mL^{-1}	[161]
		Proteins	5 ng mL^{-1}, 0.1 ng mL^{-1}	[161, 162]
		Viruses	10^7 PFU mL^{-1}	[161]
		Bacteria	5×10^8 CFU mL^{-1} 5×10^6 CFU mL^{-1}	[161]
	Porous silicon BSI	DNA	2 pmol	[163]
	BSI	Proteins	0.1 ng mL^{-1}	[164]
	Microchannel back scattering	Solutions	7×10^{-9} (RI)	[165]
		Proteins	1 fmol, 1 pmol	[166, 167]
Waveguides	Resonance mirror	Proteins	0.1 pg mm^{-2}	[168]
		Cells	10^6 ml^{-1}	[169]
	Waveguide with metallic cladding	Bacterial spores	~10^6 spores mL^{-1}	[170]
		Cells	~10 cells mm^{-2}	[171]
	Reverse-symmetry waveguide	Cells	60 cells mm^{-2}	[172]
	Waveguide with symmetric metal cladding	Solutions	2×10^{-7} (RI)	[173]
Ring resonator	Ring chip	Solutions	10^{-4}–10^{-7} (RI)	[174–177]
		DNA	~100 nmol	[178]
		Proteins	20–250 pg mm^{-2}, 0.1 ng	[174, 179, 180]
		Bacteria	10^5 CFU mL^{-1}	[178]
	Dielectric microsphere	Solutions	10^{-7} (RI)	[181]
		DNA	1 pg mm^{-2}	[182]
		Proteins	10 pg mm^{-2} (trypsin) 1 unit mL^{-1} (thrombin)	[183, 184]
		Viruses	~1 pg mm^{-2}	[185]
		Bacteria	100 CFU mm^{-2}	[186]
	Optical capillary liquid ring	Solutions	10^{-6}–10^{-7} (RI)	[187]
		DNA	4 pg mm^{-2}	[188]
		Proteins	1 pg mm^{-2}	[189]
		Viruses	1000 particles mL^{-1}	[190]
Optical fibres	Fibre Bragg grating	Solutions	10^{-6} (RI)	[191–196]
		DNA	0.7 μg mL^{-1}	[196]
	Large-period grating	Solutions	10^{-4} (RI)	[197]
		Proteins	2 μg mL^{-1}	[198]
	Nanofibres	Solutions	10^{-7} (RI)	[199, 200]
	Fabri–Perot fibre resonator	Solutions	10^{-5} (RI)	[194, 201]
		DNA	76 μmol	[202]
		Proteins	25 μg mL^{-1}	[203]
Photonic crystals	2D PC	Solutions	10^{-5} (RI)	[204, 205]
		Proteins	0.4 pg mL^{-1}	[194,201]
	2D PC resonator	Solutions	10^{-5} (RI)	[206, 207]
		Proteins	1 fg	[208]
	2D PCF	Proteins	0.15 μmol	[209]
	One-dimensional micro-cavity array based on PCF	Solutions	7×10^{-5} (RI)	[210]
	PCF	Solutions	10^{-4} (RI)	[197, 95]
		Proteins	10^{-8} mol L^{-1}	[92, 96]

Notes: SPR is the surface plasmon resonance; RI is the refractive index; BSI is the backscattering interferometer; 2D PC is the two-dimensional photonic crystal.

ing. A cell culture is applied onto a photonic crystal substrate. The growth of cells is monitored by measuring the scattering of radiation. Such a method allows the detection of even minor changes in the cell shapes and the characterisation of the introduced toxin effect.

The systems considered above make it possible to design individual label-free sensor elements of the devices, referred as 'lab-on-a-chip' (LOC). The lab-on-a-chip is a miniature system, allowing realisation of hundreds and thousands of biochemical reactions, including the stages of separation, concentration, mixing of the intermediate products, moving them into different reaction micro-chambers, and simultaneous readout of the final results aimed at the diagnostics of diseases and detection of bioterrorism agents [100]. The main advantages of LOC are the simplicity of use, high speed of assessment, minor expenditure of probed substance and reagents, and high reproducibility of results due to using standard technologies and automated equipment. In future LOCs may be used for assays that presently require specialised laboratories with expensive equipment, e.g., the point-of-care diagnostics of oncological and infectious diseases or the rapid analysis of environmental pollution in field conditions. Moreover, there is a prospect of using LOCs as micro-reactors in synthetic chemistry.

6. Photonic crystal fibres as radiation sources for biomedical applications

6.1. Optical coherence tomography

Optical coherence tomography (OCT) allows *in vivo* imaging of sub-surface tissues of the human organism with high spatial resolution [16, 101–105]. The radiation of the probing beam is focused at a biotissue, and the intensity of the signal, reflected from the tissue internal microstructure at different depths is depth-sorted and measured using interferometry under the condition that the radiation is low-coherence (broadband). Alongside with the depth scanning (A-scan) the probing beam is scanned in the lateral direction over the tissue surface (B-scan), providing the transverse image sweep that yields a 2D image. It is also possible to get 3D images.

Longitudinal (depth) and transverse (lateral) resolutions are independent quantities. The depth resolution Δz is determined by the coherence length of the light source:

$$\Delta z = \frac{2\ln 2}{\pi}\frac{\lambda_0^2}{\Delta\lambda},$$

where λ_0 is the central wavelength; $\Delta\lambda$ is the radiation bandwidth. The lateral resolution depends upon the degree of spatial coherence of the light source and the focusing optics, which should be sufficiently long-focus to provide minimal distortions in the course of the tissue depth scanning. For a Gaussian light beam with perfect spatial coherence the transverse resolution is defined as

$$\Delta x = \frac{4\lambda}{\pi}\left(\frac{f}{d}\right),$$

where f is the focus length of the lens, d is the diameter of the beam, incident on the lens. The focus depth is given by

$$b = \frac{\pi\Delta x^2}{2\lambda}.$$

The resulting data (the OCT image) form a two-dimensional pattern of backscattering (or reflection) from microscopic optical inhomogeneities (cell structures) of the biological tissue. Therefore, an OCT image actually contains information about the morphological structure of the near-surface tissues. The OCT is interesting for clinical applications for several reasons. The resolution of commercial OCT devices is 6–10 μm. This is tens or thousands times higher than the resolution of other practically used diagnostic methods (for comparison, the resolution is 240–640 μm for X-ray computer tomography, slightly less than 1 mm for magnetic resonance tomography, 2 mm for positron emission tomography, and 1–3 mm for ultrasound imaging). This implies the microscopic level of study. The information provided by OCT is intravital and exhibits not only the structure of tissues, but also the features of their functional state. Noninvasivity of the method follows from the use of low-intensity sources of radiation within the therapeutic window (0.83–1.3 μm) in the near-infrared region. Such radiation does not damage tissues and cells.

Increasing the resolution of OCT systems requires new types of radiation sources with a broad (up to hundreds of nanometres) spectrum, the coherence length of a few micrometres, and a very high degree of spatial coherence, necessary for efficient excitation of single-mode fibre interferometers, on which OCT systems are based [101–106].

The broadband optical radiation appears from the output of a PCF, excited by femtosecond laser pulses in the course of supercontinuum generation [22, 31, 59, 107–110]. The spectral width of the PCF radiation is much larger than the gain bandwidth of all crystals known at present. Figure 15 demonstrates a typical OCT image of the pig eye retina, obtained with such a light source [107].

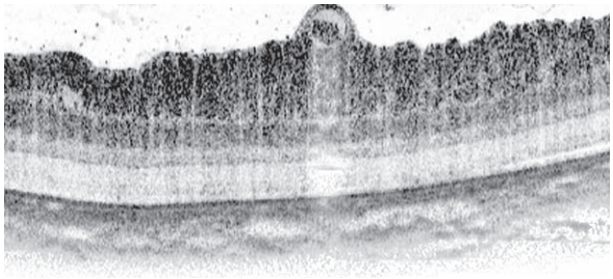

Figure 15. The image of the pig eye retina (2000×1010 pixels, 1×2 mm) [107].

The authors of [111, 112] demonstrate an OCT-aimed source of supercontinuum based on the stimulated Raman scattering in PCFs (Fig. 16) [111]. The radiation from a 10-W cw single-mode fibre Yb laser was introduced into a PCF with abnormal dispersion. As a result, the continuous spectrum was generated in the range 1090–1370 nm with the power 300 mW. The transverse resolution of the OCT in this case was 4.8 μm. As an illustration, Fig. 17 shows an *in vivo* image of the cheek skin of a golden hamster [111].

The longitudinal OCT resolution less than 1.3 μm was obtained using the PCF-generated supercontinuum radiation with the spectral band ranging from 800 to 1400 nm and the power 100 mW [113].

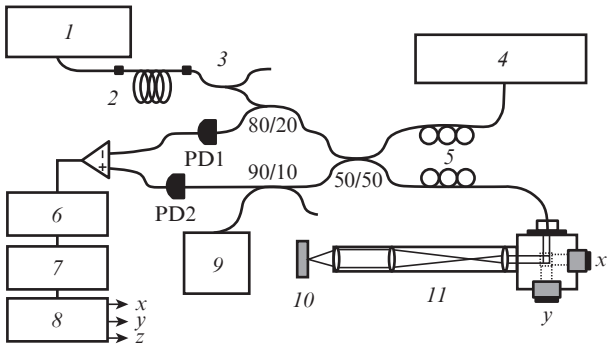

Figure 16. OCT system with a PCF source of light:
(*1*) cw ytterbium fibre laser; (*2*) PCF; (*3*) spectral multiplexer; (*4*) scanning unit in the reference arm; (*5*) polarisation controllers; (*6*) electronic detection unit; (*7*) computer; (*8*) controllers of galvanic drives for scanning along the *x*, *y*, and *z* axes; (*9*) laser beam of visible radiation for aligning the interferometer; (*10*) sample; (*11*) *xy*-scanning probe; (PD1 and PD2) photodetectors [111].

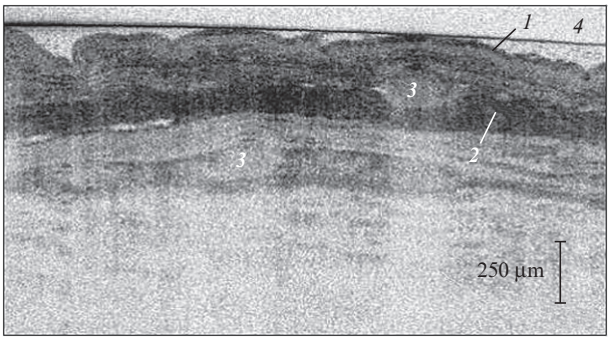

Figure 17. *In vivo* image of the cheek skin of a golden hamster with the longitudinal resolution 4.8 μm: cornified epithelial layers (*1*), muscle layers (*2*), blood vessels (*3*), cover glass (*4*) [111].

6.2. Fluorescence confocal and broadband spectroscopy and cytometry

In 2006 the papers appeared in which the light sources, generating supercontinuum, began to be used also in confocal microscopy [114]. Figure 18 shows the typical schematic diagram of a fluorescence confocal laser scanning microscope with the light source on the supercontinuum base. The generation of supercontinuum occurs in a tapered PCF. The width of the supercontinuum is 1000 nm (400 – 1400 nm) [114]. In Fig. 19 the image of a neuron-like cell is presented with the resolution of the diffraction limit order, obtained using the fluorescence confocal laser scanning microscope [114].

A year later, in 2007, the optical scheme and appropriate technique was developed for fluorescence imaging of tissues *in vivo* [115]. With the purpose of fluorescence imaging the laser radiation (1061 nm, 5 ps, 8 W) was introduced into a tapered PCF, generating supercontinuum with the lower spectral limit at the wavelength of 350 nm. In the fluorescence image of the rat tail (Fig. 20) one can easily see hair follicles, dermis, and collagen bundles [115].

In the confocal fluorescence microscope [116], proposed in 2008, the broadband radiation source was used having the central wavelength 1064 nm and the spectral range from 460 to 2000 nm. Figure 21 shows the image of the may lily

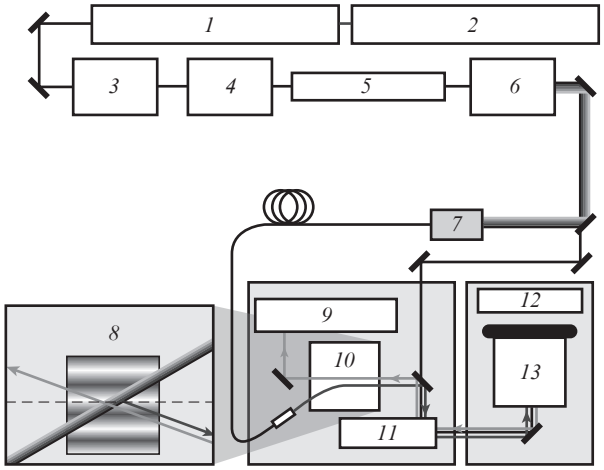

Figure 18. Confocal laser scanning microscope based on a supercontinuum source:
(*1*) Ti:sapphire laser with mode locking; (*2*) 5-W $NdYVO_4$ pump laser; (*3*) Faraday optical isolator; (*4*) objective (10×, NA = 0.3); (*5*) tapered PCF; (*6*) objective (4×, NA = 0.1); (*7*) fibre communication unit; (*8*, *10*) acousto-optical beamsplitter; (*9*) detector; (*11*) scanner; (*12*) microscope; (*13*) objective (40×, NA = 1.25) [114].

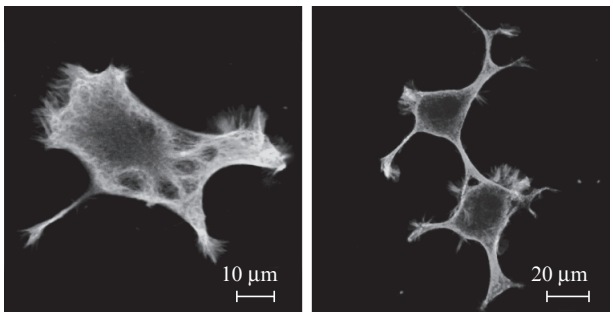

a b

Figure 19. Neuron-like cells, stained with a fluorescent dye; the fluorescence excitation occurs at the wavelengths 488 nm (a) and 543 nm (b) [114].

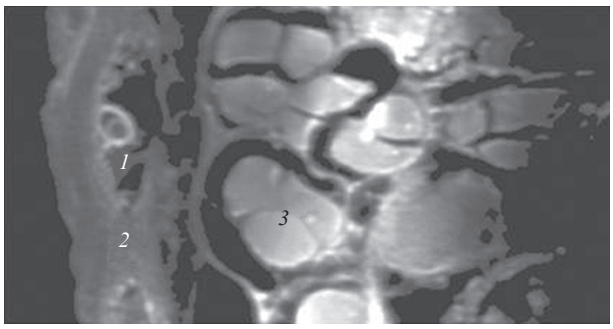

Figure 20. Rat tail image: hair follicle (*1*), dermis (*2*), collagen bundles (*3*) [115].

(*Convallaria majalis*) flower obtained using the excitation at the wavelengths 620 nm and 530 nm [116].

The excitation of fluorescent probes in flow cytometry is traditionally implemented using a few discrete wavelengths of laser radiation. The application of commercial PCF-based supercontinuum sources removes this limitation [117]. At present two companies, Fianium Ltd. (Southampton, Great

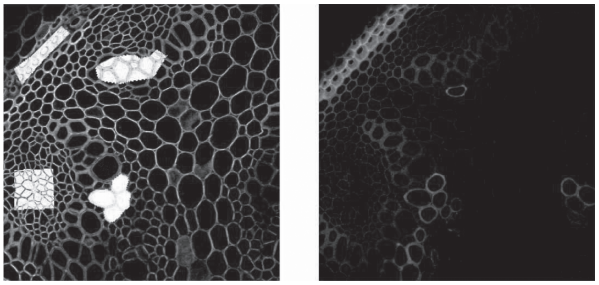

a b

Figure 21. Images of may lily (*Convallaria majalis*) obtained upon excitation at the wavelengths 620 nm (a) and 530 nm (b). The size of each image is 355×355 μm [116].

Britain) and Koheras A/S (Denmark), produce such source, having the power 5 W (460–2000 nm) and differing in the spectral distribution of intensity and signal-to-noise ratio. It is shown in Ref. [117] that the supercontinuum sources demonstrate several apparent advantages, being applied to flow cytometry. The progress in the field of semiconductor lasers allowed creation of a number of light sources with different wavelengths for using in flow cytometry; however, they still do not cover all spectral regions. Thus, the yellow-orange region (570–620 nm) remains undeveloped. Supercontinuum sources easily provide visible light of any wavelength, which makes it possible to choose fluorescent probes more accurately and removes the necessity to use multiple lasers, oscillating at different wavelengths, including even those shorter than 400 nm.

Moreover, the supercontinuum sources will allow more precise observance of the excitation conditions for particular fluorophores. This is particularly useful in such applications, as FRET (fluorescence resonance energy transfer), where the excitation/radiation wavelengths should be precisely chosen.

Thus, the design of radiation sources based on supercontinuum generation in a PCF with controlled spectral composition, coherence and power is a promising solution of the problems of optical coherence tomography, fluorescence confocal and broadband spectroscopy of molecules, and flow cytometry.

6.3. Photodynamic and photothermal therapy

Photodynamic therapy (PDT) is a method of curing oncologic and tumour diseases, some skin and numerous infection diseases, based on the use of photosensitisers and, as a rule, visible light with definite wavelength and moderate intensity [16, 118–124].

The sensitiser is usually introduced into the organism intravenously, but oral or topical administration is also possible. The substances used for PDT possess the property of selective accumulation in a tumour or any other pathological tissues (cells). The tissues affected by the pathological process are exposed to the light illumination with the wavelength, corresponding to the absorption maximum of the photosensitiser. The laser systems are used as light sources. The absorption of light quanta by the photosensitiser molecules in the presence of oxygen causes the photochemical reaction resulting in the transformation of molecular oxygen into the chemically active singlet oxygen and in the formation of multiple high-activity radicals. The singlet oxygen and the radicals cause necrosis and apoptosis of tumour cells, two basic mechanisms

Table 2. Comparative characteristics of photosensitisers

Photosensitiser	λ_{max}^{abs}/nm	W_{th}/mW cm^{-2}	η
Photofrin-2 (USA)	625±5	30–40	~0.55
Photogem (Russia)	625±5	50	~0.55
Photosense (Russia)	670±10	5	~0.3
Chlorine e6 (Russia)	660±10	10	~0.5

Notes: λ_{max}^{abs} is wavelength of the absorption maximum, W_{th} is threshold energy flow density for initiating the photodynamic effect; η is quantum yield of the singlet oxygen.

of cell death. Photodynamic therapy also violates the tumour nutrition and leads to its further destruction due to the damage of surrounding blood microvessels [125]. At present several types of photosensitisers are widely used (Table 2) [126].

To achieve high efficiency of singlet oxygen excitation one has to choose an optimal light source. This role may be played by the supercontinuum source based on the stimulated Raman scattering (SRS) in a PCF [112] that provides the sufficiently high power of generation (2.3 W). The PCF-based SRS-laser for photodynamic therapy is now developed by Russell's team [127].

The use of broadband PCF-based radiation sources in the study and practical application of photobiological and photodynamic processes in medicine is undoubtedly promising [16, 123, 124]. Note, that in many cases the multiphoton photodynamic therapy, in which the sources of femtosecond pulses are used, may appear essentially more efficient and noninvasive. For example, the new phototherapy technologies based on the photothermal action of optical radiation on tumours and microorganisms, sensitised with plasmon resonance nanoparticles, require broadband light sources [124]. Such sources are necessary also for the excitation of multicomponent photosensitisers aimed at the targeted therapy of different parts of the pathological process. This photosensitiser may be implemented as a set of dyes with different excitation wavelengths, each having his own mechanism of attaching to a pathological cell, or as a mixture of dyes with nanoparticles [128].

6.4. Laser ablation

Laser ablation is a process of laser-induced removal of substance (usually, in microscopic amounts) under the action of short pulses at wavelengths, efficiently absorbed by the substance [129]. Laser ablation with picosecond laser radiation using a hollow-core PCF was first demonstrated in [130]. The radiation, passed through the waveguide with the diameter of the hollow core 130–150 μm, was focused on the steel target; as a result, a crater with the diameter ~60 μm appeared on the target surface.

The use of laser picosecond system for ablation of tooth hard tissues is described in [38] (Fig. 22). The PCF exploited had a 2D periodic cladding, formed by the lattice of identical glass capillaries. The hollow core of the PCF was formed by extracting seven capillaries from the central part of the structure. The period of the cladding structure is ~5 μm, the diameter of the hollow core is ~13 μm. The radiation of a picosecond pulsed Nd:YAG laser (1060 nm) is passed through the PCF and focused onto the tooth surface to cause ablation of hard tissues. The radiation from the arising plasma gets back to the PCF and is transmitted to the registration system to control the ablation process. It is important that the profile of the beam outgoing from the PCF is nearly Gaussian, which

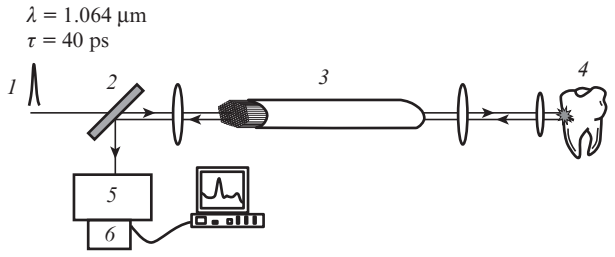

Figure 22. Schematic diagram of the experimental setup for ablation of tooth tissues:
(*1*) picosecond Nd : YAG laser pulse (40 ps, 1064 nm); (*2*) beamsplitter; (*3*) PCF with 2D periodic cladding, formed by the lattice of identical glass capillaries (the period of the cladding structure ~5 μm, the hollow core diameter ~13 μm); (*4*) tooth surface; (*5*, *6*) the ablation process control system (monochromator and CCD camera, respectively).

makes its sharp focusing onto the object possible. The radiation was focused into a spot with the diameter 15 μm on the caries-affected surface of the tooth tissue *in vitro*. In the course of ablation the emission band of calcium, contained in the tooth enamel, was found in the arising plasma radiation.

Moreover, laser ablation using PCFs has multiple potential applications in biomedicine, including the removal of haemangiomas, tattoos, etc.

7. Conclusion

The main fields of PCF application in medicine are related to the design of novel bright emitters of white light for optical coherence tomography, spectroscopy and microscopy having superhigh resolution, new types of biosensors (particularly, on the base of hollow-core PCFs) and high-intensity laser surgical and therapeutic systems, where it is necessary to transmit high-power ultrashort pulses with next-to-perfect beam shape quality for subsequent diffraction-limited focusing.

In the review the main trends and prospect of PCF applications in biomedicine are outlined. This field of research and applications is very young and, therefore, the continuing fundamental studies of PCF properties are expected to promote the discovery of novel fields of their application in biology and medicine. However, already now the PCF-based sensors demonstrate the sensitivity at the level of 10^{-7} mol L^{-1} in terms of concentration and $\sim 10^{-5}$ in terms of refractive index. The possibility to create an optical coherence tomograph with the longitudinal resolution less than 1.5 μm is demonstrated. Unique facilities are exhibited by confocal and fluorescence microscopy and spectroscopy, as well as flow cytometry, provided that the broad-band PCF-based systems are used as light sources. Such sources will find applications in the complex photodynamic therapy and photothermal therapy of cancer, involving multiple mediators of the light action with different wavelengths, as well as in the multiphoton photodynamic therapy.

The application of PCFs is promising for transmitting high-power ultrashort laser pulses without beam shape distortion and sometimes even with its correction owing to spatial filtering. These pulses are used both in nonlinear microscopy of tissues at the molecular level and for high-precision ablation of tissues and nanosurgery of cells.

In the review we used the results of the research, carried out in the International Research-Educational Centre 'Photonics' at N.G. Chernyshevsky Saratov State University (Russia), Max Born Institute of Nonlinear Optics, Institute of Applied Photonics, Institute for Scientific Instruments GmbH (Germany), and LLC SPE 'Nanostructural Glass Technology' (Saratov, Russia).

Acknowledgements. The work was partially supported by PHOTONICS4LIFEFP7-ICT-2007-2, the Ministry of Education and Science of Russia (Project Nos 1.4.09, 2.1.1/4989, and 2.2.1.1/2950), and the State Contracts of the Russian Federation (Nos 02.740.11.0484, 02.740.11.0770, and 02.740.11.0879).

References

1. Yablonovitch E. *Phys. Rev. Lett.*, **58**, 2059 (1987).
2. John S. *Phys. Rev. Lett.*, **58** (23), 2486 (1987).
3. Naniy O.E., Pavlova E.G. *Lightwave. Russian edition*, (3), 47 (2004).
4. Birks T.A., Roberts P.J., Russell P.St.J., Atkin D.M., Shepherd T.J. *Electron. Lett.*, **31**, 1941 (1995).
5. Gaponenko S.V., Rosanov I.N., Ivchenko E.L., et al. *Optika nanostruktur* (Nanostructure Optics) (Saint-Petersburg: Nedra, 2005).
6. Srinivasarao M. *Chem. Rev.*, **99**, 1935 (1999).
7. Parker A.R. *J. Opt. A, Pure Appl. Opt.*, **2**, R15 (2000).
8. Nikolaev V.A., Harwood D.M., Samsonov N.I. *Diatomovye vodorosli rannego mela* (Diatoms of Early Cretaceous) (Saint-Petersburg: Nauka, 2001).
9. Ameen D.B., Bishop M.F., McMullen T. *Biophys. J.*, **75**, 2520 (1998).
10. Maksimova I.L. *Opt. Spektrosk.*, **93** (4), 663 (2002) [*Opt. Spectrosc.*, **93** (4), 610 (2002)].
11. Fuhrman O., Lanwehr S., El Rhabi-Kucki M. *Appl. Phys.*, **78**, 257 (2004).
12. Pieranski P. *Contemp. Phys.*, **24**, 25 (1983).
13. Williams R.C., Smith K. *Nature*, **45**, 119 (1957).
14. Deniskina N.D., Kalinin D.V., Kazantseva L.K. *Blagorodnye opaly (prirodnye i sinteticheskiye)* [Noble Opals (Natural and Synthetic)] (Novosibirsk: Nauka, 1987).
15. Knight J.C., Birks T.A., Russell P.St.J., Atkin D.M. *Opt. Lett.*, **21**, 1547 (1996).
16. Tuchin V.V. *Lasery i volokonnaya optika v biomeditsinskikh issledovaniyakh* (Lasers and Fibre Optics in Biomedical Studies) (Moscow: Fizmatlit, 2010).
17. Yeh P., Yariv A., Marom E. *J. Opt. Soc. Am.*, **68**, 1196 (1978).
18. Fink Y., Ripin D.J., Fan S., Chen C., Joannopoulos J. D., Thomas E.L. *J. Lightwave Technol.*, **17** (11), 2039 (1999).
19. Brechet F., Roy P., Marcou J., Pagnoux D. *Electron. Lett.*, **36** (6), 514 (2000).
20. Knight J.C., Broeng J., Birks T.A., Russell P.St.J., Knight J.C. *Science*, **282**, 1476 (1998).
21. Cregan R.F., Mangan B.J., Knight J.C., Birks T.A., Russell P.St.J., Allen D., Roberts P.J. *Science*, **285**, 1537 (1999).
22. Russell P.S.J. *Science*, **299**, 358 (2003).
23. Knight J.C., Birks T.A., Russel P.S.J. *J. Opt. Soc. Am. A*, **15**, 748 (1998).
24. Knight J.C., Birks T.A., Cregan R.F. *Opt. Mater.*, **11**, 143 (1999).
25. Ranka J.K., Windeler R.S., Stentz A.J. *Opt. Lett.*, **25**, 25 (2000).
26. Ranka J.K., Windeler R.S., Stentz A.J. *Opt. Lett.*, **25**, 796 (2000).
27. Zheltikov A.M. *Usp. Fiz. Nauk*, **170**, 1203 (2000) [*Phys.-Usp.*, **43**, 1125 (2000)].
28. Fedotov A.B., Ivanov A.A., Alfimov M.V., Beloglazov V.I., Mel'nikov L.A., Skibina Yu.S., Zheltikov A.M. *Laser Phys.*, **10** (5), 723 (2000).
29. Beloglazov V.I., Langhoff N., Tuchin V.V., Bjeoumikhov A., Bjeoumikhova Z., Wedel R., Skibina N.B., Skibina Yu.S., Chainikov M.V. *J. X-Ray Sci. Technol.*, **13** (4), 179 (2005).
30. Wadsworth W.J., Knight J.C., Ortigosa-Blanch A., Arriaga J., Silvestre E., Russell P.St.J. *Electron. Lett.*, **36**, 53 (2000).
31. Knight J.C. *Nature*, **424**, 847 (2003).
32. Beloglazov V.I., Chainikov M.V., Skibina Yu. S., Tuchin V.V. *J. X-Ray Sci. Technol.*, **13** (4), 171 (2005).

33. Skibina J.S., Tuchin V.V., Beloglazov V.I., Skibina N.B., Chainikov M.V. *Proc. SPIE Int. Soc. Opt. Eng.*, **65351A** (2007).
34. Skibina Yu.S., Beloglazov V.I., Tuchin V.V., Chainikov M.V. *Pis'ma Zh. Tekh. Fiz*., **31** (23), 55 (2005) [*Tech. Phys. Lett*., **31** (12), 1019 (2005)].
35. Birks T.A., Knight J.C., Russell P.S.J. *Opt. Lett.*, **22**, 961 (1997).
36. Belov P.A., Simovskii K.R. *Radiotekh. Elektron.*, **49** (11) 1199 (2004) [*J. Commun. Technol. Electron.*, **49**, 1199 (2004)].
37. Luo C.L., Johnson S.G., Joannopoulos J.D., Pendry J.B. *Phys. Rev. B*, **65**, 201104 (2002).
38. Konorov S.O., Mitrokhin V.P., Fedotov A.B., Sidorov-Biryukov D.A., Beloglazov V.I., Skibina N.B., Wintner E., Scalora M., Zheltikov A.M. *Appl. Opt.*, **43** (11), 2251 (2004).
39. Broderick N.G.R., Monro T.M., Bennett P.J., Richardson D.J. *Opt. Lett.*, **24**, 1395 (1999).
40. Scalora M., Dowling J.P., Bowden C.M., Bloemer M.J. *Phys. Rev. Lett*., **73**, 1368 (1994).
41. Dowling J.P., Bowden C.M. *J. Mod. Opt.*, **41**, 345 (1994).
42. Enoch S., Tayeb G., Maystre D. *Opt. Commun.*, **161**, 171 (1999).
43. Hideo K., Takayuki K., Akihisa T., Masaya N., Toshiaki T., Takashi S., Shojiro K. *J. Lightwave Technol.*, **17** (11), 2032 (1999).
44. Konorov, S.O., Serebryannikov V.V., Ivanov A.A., Akimov D.A., Alfimov M.V., Zheltikov A.M. *Pis'ma Zh. Eksp. Teor. Fiz*., **79** (9), 499 (2004) [*JETP Lett.*, **79** (9), 395 (2004)].
45. Ouzounov D.G., Ahmad F.R., Müller D., Venkataraman N., Gallagher M.T., Thomas M.G., Silcox J., Koch K.W., Gaeta A.L. *Science*, **301**, 1702 (2003).
46. Behabid F. *Phil. Trans. R. Soc. A*, **10**, 1908 (2006).
47. Alfano R.R., Shapiro S.L. *Phys. Rev. Lett.*, **24** (11), 592 (1970).
48. Lee Smith W., Liu P., Bloembergen N. *Phys. Rev. A*, **15** (6), 2396 (1977).
49. Fork R.L., Shank C.V., Hirlimann C., Yen R. *Opt. Lett.*, **8** (1), 1 (1983).
50. Nowak G.A., Kim J., Islam M.N. *Appl. Opt.*, **38** (36), 7364 (1999).
51. Mori K., Takara H., Kawanishi S. *J. Opt. Soc. Am. B*, **18** (12), 1780 (2001).
52. Birks T.A., Wadsworth W.J., Russell P.St.J. *Opt. Lett.*, **25** (19), 1415 (2000).
53. Husakou V.A., Herrmann J. *Phys. Rev. Lett.*, **87**, 203901 (2001).
54. Herrmann J., Griebner U., Zhavoronkov N., Husakou A., Nickel D., Knight J.C., Wadsworth W.J., Russell P.St.J., Korn G. *Phys. Rev. Lett.*, **88**, 173901 (2002).
55. Gaeta L.A. *Opt.Lett.*, **27**, 924 (2002).
56. Skryabin D.V., Gorbach A.V. *Rev. Mod. Phys.*, **82**, 1287 (2010).
57. Malomed B.A. *Kontrol' solitonov v periodicheskikh sredakh* (Control of Solitons in Periodic Media) (Moscow: Fizmatlit, 2009).
58. Kudryashov N.A., Zargarian E.D. *Inzh.-Fiz. Zhurn.*, **71**, 1 (1998).
59. Glas P., Fischer D., Steinmeyer G., Husakou A., Herrmann J., Iliew R., Skibina N.B., Beloglasov V.I., Skibina J.S. *Appl. Phys. B*, **81**, 209 (2005).
60. Kafka J.D., Watts M.L., Pieterse J.-W.J. *J. Quantum Electron.*, **28** (10), 2151 (1992).
61. Ravi Kumar V.V., George A., Reeves W., Knight J., Russell P., Omenetto F., Taylor A. *Opt. Express*, **10** (25), 1520 (2002).
62. Buczynski R., Bookey H.T., Pysz D. *Laser Phys. Lett.*, **7** (9), 666 (2010).
63. Skibina J.S., Iliew R., Bethge J., Bock M., Fischer D., Beloglasov V.I., Wedell R., Steinmeyer G. *Nature Photonics*, **2**, 679 (2008).
64. Bethge J., Le T., Skibina J., Stingl A., Steinmeyer G. *Techn. Dig. Conf. Lasers and Electrooptics* (New York: OSA, 2010) paper CMU5.
65. Hartl I., Li X.D., Chudoba C., Ghanta R.K., Ko T.H., Fujimoto J.G., Ranka J.K., Windeler R.S. *Opt.Lett*., **26**, 608 (2001).
66. Holzwarth R., Zimmermann M., Udem Th., Hánsch T.W., Russbüldt P., Gäbel K., Poprawe R., Knight J.C., Wadsworth W.J., Russell P.St.J. *Opt. Lett.*, **26** (17), 1376 (2001).
67. Holzwarth R., Udem Th., Hänsch T.W., Knight J.C., Wadsworth W.J., Russell P.St.J. *Phys. Rev. Lett.*, **85**, 2264 (2000).
68. Reichert J., Niering M., Holzwarth R., Weitz M., Udem Th., Hänsch T.W. *Phys. Rev. Lett.*, **84**, 3232 (2000).
69. Hollberg L., Oates C.W., Curtis E.A., Ivanov E.N., Diddams S.A., Udem T., Robinson H.G., Bergquist J.C., Rafac R.J., Itano W.M., Drullinger R.E., Wineland D.J. *IEEE J. Quantum Electron.*, **37**, 1502 (2001).
70. Udem Th., Reichert J., Holzwarth R., Hänsch T.W. *Opt. Lett.*, **24** (13), 881 (1999).
71. Udem Th., Reichert J., Holzwarth R., Hänsch T.W. *Phys. Rev. Lett.*, **82** (18), 3568 (1999).
72. Brackett C.A. *IEEE J. Sel. Areas Commun.*, **8** (6), 948 (1990).
73. Takara H. *Electron. Lett.*, **36** (25), 2089 (2000).
74. Mori K., Morioka T., Saruwatari M. *IEEE Trans. Instrum. Meas.*, **44**, 712 (1995).
75. Cundiff S.T., Ye J., Hall J.L. *Rev. Sci. Instrum.*, **72** (10), 3749 (2001).
76. Yusoff Z. *Opt. Lett.*, **27**, 424 (2002).
77. Zheltikov A.M. *Usp. Fiz. Nauk*, **176**, 623 (2006) [*Phys.-Usp.*, **49**, 605 (2006)].
78. Zheltikov A.M. *Usp. Fiz. Nauk*, **177**, 737 (2007) [*Phys.-Usp.*, **50**, 705 (2007)].
79. Pavone F.S. (Ed.) *Laser Imaging and Manipulation in Cell Biology* (Weinheim: Wiley-VCH Verlag GmbH & Co., 2010).
80. Varfolomeyev S.D., Evdokimov Yu.N., Ostrovsky M.A. *Vestn. RAMN*, **70** (1), 21 (2000).
81. Ivanov A.V., Mushta V.M., Pevgov V.G. *Ross. Bioterapevt. Zh*., **6** (1), 74 (2007).
82. Samudrala P. *Master's thesis* (Morgantown, West Virginia University, 2006).
83. Leung A., Shankar P. M., Mutharasan R. *Sensors and Actuators B*, **125**, 688 (2007).
84. Yuan Y., Yi B., Xiao J., Li Z. *Proc. Int. Conf. on Bioinformatics and Biomedical Engineering* (Wuhan, China, 2007) p. 1043.
85. Hoa X.D., Kirk A.G., Tabrizian M. *Biosensors and Bioelectronics*, **23** (2), 151 (2007).
86. Homola J., Yee S.S., Gauglitz G. *Sensors and Actuators B*, **54**, 3, (1999).
87. Lassiter J.B., Knight M.W., Mirin N.A. *Nano Lett.*, **9** (12), 4326 (2009).
88. Hoo Y.L., Jin W., Ho H.L., Wang D.N., Windeler R.S. *Opt. Eng.*, **41** (1), 8 (2002).
89. Myaing M.T., Ye J.Y., Norris T.B., Thomas T., Baker J., Wadsworth W.J., Bouwmans G., Knight J.C., Russell P.S.J. *Opt. Lett.*, **28**, 1224 (2003).
90. Jensen J., Hoiby P., Emiliyanov G., Bang O., Pedersen L., Bjarklev A. *Opt. Express*, **13** (15), 5883 (2005).
91. Konorov S.O. Zheltikov A., Scalora M. *Opt. Express*, **13** (9), 3454 (2005).
92. Tuchin V.V., Skibina Yu.S., Beloglazov V.I., Chainikov M.V., Skibina N.B., Mikhailova N.A., Zhestkov P.M., Silokhin I.Yu. *Pis'ma Zh. Tekh. Fiz*., **34** (15), 63 (2008) [*Tech. Phys. Lett.*, **34** (8), 663 (2008)].
93. Zheng H. *J. Innovative Opt. Health Sci.*, **2** (1), 73 (2009).
94. http://www.irocmedical.com.
95. Malinin A.V., Zanishevskaja A.A., Skibina Yu.S., Silokhin I.Yu., Tuchin V.V., Dubrovskiy V.A., Dolmashkin A.A. *Proc. SPIE Int. Soc. Opt. Eng.*, **7898**, 46 (2011).
96. Malinin A.V., Skibina Yu.S., Mikhailova N.A., Silokhin I.Yu., Chainikov M.V. *Pis'ma Zh. Tekh. Fiz*., **36** (8), 33 (2010) [*Tech. Phys. Lett*., **36** (4) 362 (2010)].
97. Malinin A.V., Skibina Yu.S., Tuchin V.V., Chainikov M.V., Beloglazov V.I., Silokhin I.Yu., Zanishevskaya A.A., Dubrovskii V.A., Dolmashkin A.A. *Kvantovaya Elektron.*, **41**, 302 (2011) [*Quantum Electron*., **41**, 302 (2011)].
98. Xudong F. *Anal. Chim. Acta*, **620**, 8 (2008).
99. Schwartz M.P., Derfus A.M., Alvarez S.D., Bhatia S.N., Sailor M.J. *Langmuir*, **22**, 7084 (2006).
100. Mirzabekov A.D. *Vestnik Ross. Akad. Nauk*, **73** (5), 412 (2003).
101. Zimnyakov D.A., Tuchin V.V. *Kvantovaya Elektron*., **32** (10), 849 (2002) [*Quantum Electron*., **32** (10), 849 (2002)].
102. Fercher A.F., Drexler W., Hitzenberger C.K. *Rep. Progr. Phys.*, **66**, 239 (2003).
103. Gladkova N.D. *Opticheskaya kogerentnaya tomografiya v ryadu metodov meditsinskoy vizualiztsii* (Optical Coherence Tomography among the Methods of Medical Visualisation) (Nizhnii Novgorod: Institute of Applied Physics, RAS, 2005).
104. Gladkova N.D., Shakhova N.M., Sergeev A.M. (Eds) *Rukovodstvo po opticheskoy kogerentnoy tomografii* (Optical Coherence Tomography Manual) (Moscow: Fizmatlit, 2007).
105. Drexler W., Fujimoto J.G. *Optical Coherence Tomography: Technology and Applications* (Berlin: Springer, 2008).

106. Kowalevicz A., Ko T., Hartl I., Fujimoto J., Pollnau M., Salath R. *Opt. Express*, **10** (7), 349 (2002).
107. Povazay B., Bizheva K., Hermann B., Unterhuber A. *Opt. Express*, **11** (17), 1980 (2003).
108. Ranka J.K., Windeler R.S., Stentz A. *J. Opt. Lett*., **25**, 25 (2000).
109. Zheltikov A.M. *Optika mikrostrukturirovannykh volokon* (Optics of Microstructured Fibres) (Moscow: Nauka, 2004).
110. Zheltikov A.M. *Usp. Fiz. Nauk*, **174**, 73 (2004) [*Phys.-Usp*., **47**, 69 (2004)].
111. Hsiung P.-L., Chen Y., Ko T., Fujimoto J., Matos C., Popov S., Taylor J., Gapontsev V. *Opt. Express*, **12** (22), 5287 (2004).
112. Avdokhin A.V., Popov S.V., Taylor J.R. *Opt. Lett.*, **28** (15), 1353 (2002).
113. Wang Y., Zhao Y., Nelson J. S., Chen Z. *Opt. Lett.*, **28** (3), 182 (2003).
114. http://www.optoiq.com.
115. Owen D., Auksorius E. *Opt. Lett.*, **32** (23), 3408 (2007).
116. Schlachter S., Elder A. *Microscopy and Analysis*, **22** (3), 11 (2008).
117. Telford W.G., Subach F.V. *Cytometry A*, **75A**, 450, (2009).
118. Vladimirov Yu.A, Potapenko A.Ya. *Fiziko-khimicheskiye osnovy fotobiologicheskikh protsessov: uchebnik dlya vuzov* (Physicochemical Fundamentals of Photobiological Processes: A University Textbook) (M.: Drofa, 2006).
119. Krasnovsky A.A. *Biofiz.*, **49** (2), 305 (2004) [*Biophys.*, **49** (2), 289 (2004)].
120. Meerovich G.A., Stratonnikov A.A., Loschenov V.B., Kogan E.A., Ladskikh O.P., Lukyanets E.A., Vorozhtsov G.N., Pal'tsev M.A. *Laz. Med*., **4** (4), 19 (2000).
121. Stranadko E.F., Titova V.A., Ryabov M.V., Petrovskii V.Yu. *Laz. Med*., **10** (3), 41 (2006).
122. Tolstykh P.I., Klebanov G.I., Shekhter A.B., Tolstykh M.P. *Antioksidanty i lazernoye izlucheniye v terapii ran i troficheskikh yazv* (Antioxidants and Laser Radiation in Therapy of Wounds and Trophic Ulcers) (Moscow: "Eko" Publishing House, 2002).
123. Hamblin M., Mros P. (Eds) *Advances in Photodynamic Therapy: Basic, Translational and Clinical* (Boston–London: Artec House, 2008).
124. Tuchin V.V. (Ed.) *Handbook of Photonics for Biomedical Science* (London: CRC Press, Taylor & Francis Group, 2010).
125. Loschenov V.B., Konov V.I., Prokhorov A.M. *Laser Phys.*, **10** (6), 1188 (2000).
126. Zhorina L.V., Zmievskoy G.N. *Osnovy vzaimodeystviya fizicheskikh poley s biologicheskimi ob'ektami* (Fundamentals of Interaction of Physical Fields with Biological Objects) (Moscow: Bauman MSTU Publishers, 2006).
127. http://www.nextgen-pcf.eu.
128. Tuchina E.S., Tuchin V.V., Khlebtsov B.N., Khlebtsov N.G. *Kvantovaya Elektron*., **41**, 354 (2011) [*Quantum Electron*., **41**, 354 (2011)].
129. Anisimov S.I., Luk'yanchuk B.S. *Usp. Fiz. Nauk*, **172** (3), 301 (2002) [*Phys.-Usp.*, 45 (3), 293 (2002)].
130. Konorov S.O., Fedotov A.B., Beloglazov V.I., Skibina N.B., Shcherbakov A.V., Wintner E., Zheltikov A.M. *Laser Phys.*, **13** (4), 652 (2003).
131. Tao N.J., Boussaad S., Huang W. L., Arechabaleta R. A., D'Agnese J. *Rev. Sci. Instrum.*, **70**, 4656 (1999).
132. Slavik R., Homola J., Ctyroky J. *Sens. Actuators B Chem.*, **54**, 74 (1999).
133. Monzon-Hernandez D., Villatoro J. *Sens. Actuators B Chem.*, **115**, 227 (2006).
134. Suzuki A., Kunihara K., Kobayashi M., Tabata S. *Sens. Actuators B Chem*., **106**, 383 (2005).
135. Chien F.C., Lin C.Y., Yih J.N., Lee K.L., Chang C.W., Wei P.K., Sun C.C., Chen S.J. *Biosens. Bioelectron.*, **22**, 2737 (2007).
136. Dostalek J., Homola J., Miler M. *Sens. Actuators B Chem.*, **107**, 154 (2005).
137. Nenninger G.G., Tobiska P., Homola J., Yee S.S. *Sens. Actuators B Chem.*, **74**, 145 (2001).
138. Slavik R., Homola J. *Sens. Actuators B Chem.*, **123**, 10 (2007).
139. Shumaker-Parry J.S., Campbell C.T. *Anal. Chem.*, **76**, 907 (2004).
140. Zybin A., Grunwald C., Mirsky V.M., Kuhlmann J., Wolfbeis O.S., Niemas K. *Anal. Chem.*, **77**, 2393 (2005).
141. Piliarik M., Vaisocherova H., Homola J. *Biosens. Bioelectron.*, **20**, 2104 (2005).
142. Chinowsky T.M., Grow M.S., Johnston K.S., Nelson K., Edwards T., Fu E., Yager P. *Biosens. Bioelectron.*, **22**, 2208 (2007).
143. Lee H.J., Nedelkov D., Corn R.M. *Anal. Chem.*, **78**, 6504 (2006).
144. Kuo W.-C., Chou C. *Opt. Lett.*, **28**, 1329 (2003).
145. Law W.-C., Markowicz P., Yong K.-T., Roy I., Baev A., Patskovsky S., Kabashin A.V., Ho H.-P., Prasad P.N. *Biosens. Bioelectron.*, **23**, 627 (2007).
146. He L., Musick M.D., Nicewarner S.R. *J. Am. Chem. Soc.*, **122**, 9071 (2000).
147. Nelson B.P., Grimsrud T.E., Liles M.R. *Anal. Chem.*, **73**, 1 (2001).
148. Song F., Zhou F., Wang J., Tao N., Lin J. *Nucleic Acids Res.*, **30**, e72 (2002).
149. Yao X., Li X., Toledo F., Zurita-Lopez C. *Anal. Biochem.*, **354**, 220 (2006).
150. Besselink G.A.J., Kooyman R.P.H., van Os P.J.H.J., Engbers G. H.M., Schasfoort R.B.M. *Anal. Biochem*., **333**, 165 (2004).
151. Chung J.W., Bernhardt R., Pyun J.C. *Sens. Actuators B Chem.*, **118**, 28 (2006).
152. Teramura Y., Iwata H. *Anal. Biochem.*, **365**, 201 (2007).
153. Taylor A.D., Yu Q., Chen S., Homola J., Jiang S. *Sens. Actuators B Chem*., **107**, 202 (2005).
154. Oh B.-K., Kim Y.-K., Park K.W., Lee W.H., Choi J.-W. *Biosens. Bioelectron*., **19**, 1497 (2004).
155. Waswa J.W., Debroy C., Irudayaraj J. *Food Process Eng*., **29**, 373 (2006).
156. Heideman R.G., Lambeck P.V. *Sens. Actuators B Chem.*, **61**, 100 (1999).
157. Weisser M., Menges B., Mittler-Neher S. *Biosens. Bioelectron*., **14**, 405 (1999).
158. Brandenburg A. *Sens. Actuators B Chem.*, **39**, 266 (1997).
159. Ymeti A., Kanger J.S., Greve J., Lambeck P.V., Wijn R., Heideman R.G. *Appl. Opt.*, **42**, 5649 (2003).
160. Ymeti A., Greve J., Lambeck P.V., Wink T., van Hovell S., Beumer T.A.M., Wijn R.R., Heideman R.G., Subramaniam V. *Nano Lett*., **7**, 394 (2007).
161. Schneider B.H., Edwards J.G. *Clin. Chem.*, **43**, 1757 (1997).
162. Schneider B.H., Dickinson E.L., Vach M.D., Hoijer J.V., Howard L.V. *Biosens. Bioelectron*., **15**, 13 (2000).
163. Lin V.S.-Y., Motesharei K., Dancil K.P.S., Sailor M.J. *Science*, **278**, 840 (1997).
164. Zhao M., Nolte D., Cho W., Regnier F. *Clin. Chem.*, **52**, 2135 (2006).
165. Wang Z., Bornhop D.J. *Anal. Chem*., **77**, 7872 (2005).
166. Markov D.A., Swinney K., Bornhop D.J. *J. Am. Chem. Soc.*, **126**, 16659 (2004).
167. Bornhop D.J., Latham C., Kussrow A. *Science*, **317**, 1732 (2007).
168. http://www.neosensors.com.
169. Watts H.J., Lowe C.R. *Anal. Chem.*, **66**, 2465 (1994).
170. Zourob M., Mohr S., Brown B.J.T., Fielden P.R. *Anal. Chem.*, **77**, 232 (2005).
171. Skivesen N., Horvath R, Thinggaard S. *Biosens. Bioelectron.*, **22**, 1282 (2007).
172. Horvath R., Fricsovszky G., Papp E. *Opt. Lett.*, **28**, 1233 (2003).
173. Wang Y., Li H., Cao Z., Yu T. *Appl. Phys. Lett.*, **92**, 061117 (2008).
174. Chao C.-Y., Fung W., Guo L.J. *IEEE J. Sel. Top. Quantum Electron.*, **12**, 134 (2006).
175. Yalcin A., Popat K.C., Aldridge J.C. *IEEE J. Sel. Top. Quantum Electron*., **12**, 148 (2006).
176. De Vos K., Bartolozzi I., Schacht E., Bienstman P., Baets R. *Opt. Express*, **15**, 7610 (2007).
177. Barrios C.A., Gylfason K. B., Sánchez B., Griol A., Sohlström H., Holgado M., Casquel R. *Opt. Lett.*, **32**, 3080 (2007).
178. Ramachandran A., Wang S., Clarke J. *Biosens. Bioelectron.*, **23**, 939 (2008).
179. Ksendzov A., Lin Y. *Opt. Lett.*, **30**, 3344 (2005).
180. Barrios C.A., Bañuls M.J., González-Pedro V., Kristinn B.G., Benito S., Maquieira A., Sohlström H., Holgado M., Casquel R. *Opt. Lett*., **33**, 708 (2008).
181. Hanumegowda N.M., White I.M., Oveys H., Fan X. *Sens. Lett.*, **3**, 315 (2005).
182. Vollmer F., Arnold S., Braun D., Teraoka I., Libchaber A. *Biophys. J.*, **85**, 1974 (2003).
183. Hanumegowda N.M., Stica C.J., Patel B.C. *Appl. Phys. Lett.*, **87**, 201107 (2005).
184. Zhu H., Suter J.D., White I.M. *Sensors*, **6**, 785 (2006).
185. Arnold S., Ramjit R., Keng D., Kolchenko V. *Faraday Discuss.*, **137**, 65 (2008).
186. Ren H.-C., Vollmer F., Arnold S. *Opt. Express*, **15**, 17410 (2007).

187. Fan X., White I.M., Zhu H., Suter J.D., Oveys H. *SPIE Laser Resonators and Beam Control X*, **6452** (2007).
188. Suter J.D., White I.M., Zhu H., Shi H., Caldwell C.W., Fan X. *Biosens. Bioelectron.*, **23**, 1003 (2008).
189. Zhu H., White I.M., Suter J.D., Dale P.S., Fan X. *Opt. Express*, **15**, 9139 (2007).
190. Zhu H., White I.M., Suter J.D., Fan X. *Analyst*, **132**, 356 (2008).
191. Schroeder K., Ecke W., Mueller R., Willsch R., Andreev A. *Meas. Sci. Technol.*, **12**, 757 (2001).
192. Smith K.H., Ipson B.L., Lowder T.L., Hawkins A.R., Selfridge R.H., Schultz S.M. *Appl. Opt.*, **45**, 1669 (2006).
193. Lowder T.L., Gordon J.D., Schultz S.M., Selfridge R.H. *Opt. Lett.*, **32**, 2525 (2007).
194. Liang W., Huang Y., Xu Y., Lee R.K. *Appl. Phys. Lett.*, **86**, 151122 (2005).
195. Chryssis A.N., Lee S.M., Lee S.B. *IEEE Photonics Technol. Lett.*, **17**, 1253 (2005).
196. Chryssis A.N., Saini S.S., Lee S.M., Yi H., Bentley W.E., Dagenais M. *IEEE J. Sel. Top. Quantum Electron.*, **11**, 864 (2005).
197. Rindorf L., Rindorf L., Jensen J.B., Dufva M., Bang O. *Opt. Express*, **14**, 8224 (2006).
198. DeLisa M.P., Zhang Z., Shiloach M., Pilevar S. *Anal. Chem.*, **72**, 2895 (2000).
199. Xu F., Horak P., Brambilla G. *Opt. Express*, **15**, 9385 (2007).
200. Tazawa H., Kanie T., Katayama M. *Appl. Phys. Lett.*, **91**, 113901 (2007).
201. Wei T., Han Y., Tsai H.-L., Xiao H. *Opt. Lett.*, **33**, 536 (2008).
202. Wang X., Xu J., Cooper K., Wang A., Xu J., Wang Z., Zhang Y., Tu J. *Appl. Phys. Lett.*, **89**, 163901 (2006).
203. Zhang Y., Shibru H., Cooper K.L., Wang A.B. *Opt. Lett.*, **30**, 1021 (2005).
204. Cunningham B., Li P., Lin Bo, Pepper J. *Sens. Actuators B Chem.*, **81**, 316 (2002).
205. Li P.Y., Lin Bo, Gerstenmaier J., Cunningham B.T. *Sens. Actuators B Chem.*, **99**, 6 (2004).
206. Loncar M., Scherer A., Qiu Y. *Appl. Phys. Lett.*, **82**, 4648 (2003).
207. Chow E., Grot A., Mirkarimi L.W. *Opt. Lett.*, **29**, 1093 (2004).
208. Lee M.R., Fauchet P.M. *Opt. Express*, **15**, 4530 (2007).
209. Skivesen N., Tetu A., Kristensen M., Kjems J., Frandsen L.H., Borel P.I. *Opt. Express*, **15**, 3169 (2007).
210. Mandal S., Erickson D. *Opt. Express*, **16**, 1623 (2008).